Nucleic Acids Research, 2026, **54**, gkag003
https://doi.org/10.1093/nar/gkag003
Chemical Biology and Nucleic Acid Chemistry

The two-step purification method ViREn identifies a single NSUN6-mediated 5-methylcytosine modification promoting dengue virus RNA genome turnover

Chia Ching Wu[1], Isabel S. Naarmann-de Vries[2,3], Jonas Hartmann[1], Zarina Nidoieva[4], Kevin Kopietz[4], Virginie Marchand[5,6], Zeynep Özrendeci[4], Doris Lindner[7,8], Sophia Schelchshorn[1], Sophia Flad[9], Michaela Frye[9], F. Nina Papavasiliou[10], Tanja Schirmeister[4], Georg Stoecklin[7,8], Johanna Schott[7,8], Yuri Motorin[5,6], Francesca Tuorto[7,8], Christoph Dieterich[2,3], Mark Helm[4], Alessia Ruggieri[1,*]

[1]Department of Infectious Diseases, Molecular Virology, Center for Integrative Infectious Disease Research, Heidelberg University, Medical Faculty Heidelberg, 69120 Heidelberg, Germany
[2]Klaus Tschira Institute for Integrative Computational Cardiology, Heidelberg University, Medical Faculty Heidelberg, 69120 Heidelberg, Germany
[3]German Centre for Cardiovascular Research (DZHK)-Partner Site Heidelberg/Mannheim, 69120 Heidelberg, Germany
[4]Institute of Pharmaceutical and Biomedical Sciences, Johannes Gutenberg University Mainz, 55128 Mainz, Germany
[5]Université de Lorraine, SMP IBSLor, EpiRNA-Seq Core Facility, 54000 Nancy, France
[6]Université de Lorraine, CNRS, UMR7365 IMoPA, 54000 Nancy, France
[7]Division of Biochemistry, Mannheim Institute for Innate Immunoscience (MI3) and Mannheim Cancer Center (MCC), Heidelberg University, Medical Faculty Mannheim, 68167 Mannheim, Germany
[8]Center for Molecular Biology of Heidelberg University (ZMBH), German Cancer Research Center (DKFZ)-ZMBH Alliance, 69120 Heidelberg, Germany
[9]Division of Mechanisms Regulating Gene Expression, German Cancer Research Center—Deutsches Krebsforschungszentrum (DKFZ), 69120 Heidelberg, Germany
[10]Division of Immune Diversity, German Cancer Research Center—Deutsches Krebsforschungszentrum (DKFZ), 69120 Heidelberg, Germany
*To whom correspondence should be addressed. Email: alessia.ruggieri@med.uni-heidelberg.de

Abstract

Chemical modifications on cellular and viral RNAs are new layers of post-transcriptional regulation of cellular processes, including RNA stability and translation. Although advances in analytical methods have improved the detection of RNA modifications, precise mapping at single-base resolution remains challenging. Requirements for sensitivity and purity limit accuracy and reproducibility, especially for low abundant viral RNAs extracted from infected cells. Here, we report a two-step method, ViREn, for the enrichment of the genomic RNA (gRNA) of dengue virus (DENV), a positive-sense single-stranded RNA virus. This approach enabled the preparation of gRNA with significantly increased purity and led to the identification of a single high-confidence 5-methylcytosine (m^5C) site in DENV gRNA at position 1218. This finding was orthogonally validated by Illumina-based bisulfite sequencing and by Nanopore Oxford Technologies direct RNA sequencing. Strikingly, m^5C1218 was detected exclusively in gRNA extracted from infected cells but not in gRNA extracted from viral particles. We identified NSUN6 as the host methyltransferase catalyzing this modification and demonstrated a role for m^5C in regulating DENV gRNA turnover. ViREn thus enables the mapping of m^5C on low-abundance viral gRNA with unprecedented precision and sensitivity and facilitates future mechanistic studies into the role of RNA modifications in virus replication.

Graphical abstract

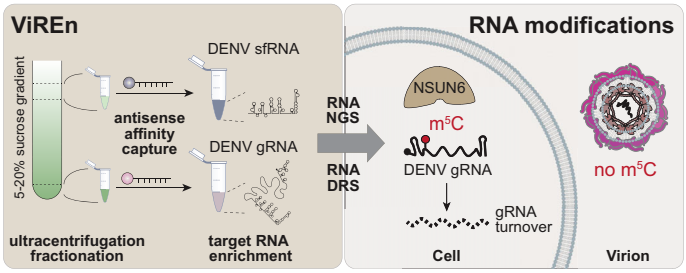

Received: April 18, 2025. **Revised:** December 15, 2025. **Accepted:** December 23, 2025

Introduction

Several classes of coding and noncoding RNA molecules carry chemical modifications [1–3], including messenger RNAs (mRNAs) at low abundance [4]. Modifications can affect RNA structure and regulate cellular processes, including splicing, nuclear export, stability, and translation [5]. Recent advances in analytical methods have improved the sensitivity for detection of RNA modifications, e.g. using liquid chromatography–tandem mass spectrometry (LC-MS/MS) [6]. Similarly, the use of antibody-enriched or chemical-treated RNA in combination with RNA sequencing (RNA-seq) has improved the resolution and mapping of prevalent RNA modifications, such as N^6-methyladenosine (m^6A) and 5-methylcytosine (m^5C), at single-base resolution [7]. However, these approaches still suffer from several disadvantages that affect accuracy and reproducibility, including non-specific binding of antibodies, incomplete chemical conversion in the case of chemical treatments, low sensitivity for rare modifications, and high material requirements. Apart from RNA-seq, the development of direct RNA sequencing (DRS) by Nanopore Oxford Technologies (ONT) has paved the way for detecting RNA modifications in native single RNA molecules, significantly contributing to our understanding of the dynamic epitranscriptome [8, 9].

These advances have also reinvigorated the search for RNA modifications in viral RNAs, particularly in the genome of positive-sense (+) single-stranded (ss) RNA viruses, since modifications may directly influence their replication. The combined use of antibody-based purification and RNA-seq has allowed the identification of multiple m^6A-modified sites within the genome of several *Flaviviridae*, including dengue virus (DENV), Zika virus, yellow fever virus, West Nile virus, and hepatitis C virus (HCV), suggesting a potentially conserved function across this virus family [10, 11]. In comparison to m^6A, less is known about m^5C in the genome of *Flaviviridae*, probably due to its relatively low abundance. Furthermore, over 30 additional types of RNA modifications were identified in the genomic RNAs (gRNAs) of several RNA viruses by RNA affinity capture coupled to LC-MS/MS [12]. However, some of the results have proven poorly reproducible, highlighting methodological shortcomings mainly due to low viral RNA abundance and contaminations by residual cellular RNAs such as highly modified transfer RNAs (tRNAs) and ribosomal RNAs (rRNAs). This has led to controversy over the positional mapping of modifications and underscored the necessity for orthogonal and functional validation [13, 14].

DENV is a mosquito-borne human pathogen and a major public health burden. Dengue cases have seen an unprecedented increase in 2024, reaching 14 million infections and >10 000 dengue-related deaths worldwide (ECDC Dengue Case Notification Rate, Jan–Dec 2024). The DENV gRNA is ~10.7 kilobases long, flanked by highly structured untranslated regions (UTRs) at the 5′ and 3′ ends. The open reading frame of DENV gRNA encodes a single polyprotein that is both co- and post-translationally cleaved to yield three structural and seven non-structural (NS) proteins involved in viral particle production and replication, respectively. The gRNA is capped at the 5′ end by the viral RNA-dependent RNA polymerase NS5 but lacks a polyadenylated tail at its 3′ end [15]. The DENV replication cycle is exclusively cytoplasmic. During infection, the 5′ portion of the gRNA is degraded by the cellular 5′–3′ exonuclease XRN1, an essential component of the decapping-dependent RNA decay pathway [16]. XRN1 stalls at compact RNA folds in the gRNA 3′UTR, generating small noncoding RNAs called subgenomic flaviviral RNA (sfRNA) [17, 18]. sfRNA accumulates in the cytosol during infection as part of the viral strategy, where it counteracts cellular antiviral responses in mosquito and vertebrate hosts [19–23] and contributes to viral pathogenicity [22–24].

Accurate identification and mapping of modified ribonucleotides have improved with advanced sequencing methods and basecalling algorithms. Nevertheless, precise detection of RNA modifications remains affected by sequencing depth, the design of appropriate controls for algorithm training, and the number of biological replicates analyzed [25]. Low purity and yield of viral RNA isolation protocols are the main obstacles to increasing sequencing depth. To overcome this limitation, we developed a viral RNA enrichment method—called ViREn—for the in-depth sequencing and mapping of DENV gRNA modifications. ViREn is a two-step approach that separates DENV RNAs (gRNA and sfRNA) from most other cellular RNAs based on (i) their sedimentation coefficient in sucrose gradients and (ii) sequence-specific affinity capture. Using ViREn in combination with Illumina-based bisulfite sequencing (BSSeq) and DRS, we identified a single m^5C site at position 1218 of the DENV gRNA with high confidence. This modification, exclusive to gRNA extracted from infected cells and undetectable in gRNA extracted from viral particles, is catalyzed by the cellular methyltransferase Nol1/Nop2/SUN 6 (NSUN6) and promotes DENV gRNA turnover.

Materials and methods

Cells

Huh7 cells, Huh7 NT cells, and Huh7 NSUN6 KO cells were maintained at 37°C and 5% CO_2 in Dulbecco's modified Eagle medium (DMEM, Gibco) supplemented with 10% fetal calf serum (Capricorn), 1% nonessential amino acids, 100 U/ml penicillin, and 100 µg/ml streptomycin (all from Gibco). BHK-21 cells (used for virus stock production) were maintained in Glasgow Minimum Essential Medium (Gibco) supplemented with 5% FCS (Capricorn), 10% tryptose phosphate broth (Sigma–Aldrich), 2 mM L-glutamine, 100 U/ml penicillin, and 100 µg/ml streptomycin (all from GIBCO).

Plasmids

The following plasmids were used and described elsewhere: pDVWSK601, harboring the full-length complementary DNA (cDNA) of DENV type 2 New Guinea C [26] (kindly provided by Andrew Davidson, University of Bristol, England), was used for production of DENV2 viral stocks and *in vitro* synthesis of unmethylated control RNAs for BSSeq and DRS. pDVWSK601 LucUbi [27], harboring DENV NGC firefly luciferase reporter virus, was used for the characterization of DENV replication in Huh7 NSUN6 KO cells.

The plasmid pDVWSK601 C1218T was generated using pDVWSK601 as a template. The point mutation was introduced by site-directed mutagenesis using overlap extension polymerase chain reaction (PCR). Two sets of degenerate PCR primers were: DENV-E_BsrGI_For: 5′-AGAGAAACCGCGTGTCGACTGTACAACAGCTGACAAAG-3′ and DENV-E_C1218T_Rev: 5′-CATCCTCTGTCCACCATGGAATCTTTGCAGACGAACCT-3′; DENV-

E_C1218T_For: 5′-AGGTTCGTCTGCAAACATTCCATG GTGGACAGAGGATG-3′ and DENV-E_NheI_Rev: 5′-AGCTTTCTGGATAGCTGAAGCTTTGAAGGGGATTCTG G-3′. Amplicons were amplified using Phusion DNA polymerase (New England Biolabs, NEB), separated by agarose gel electrophoresis, and purified from the gel using NucleoSpin Gel and PCR Clean-up (Macherey-Nagel). Equal amounts of each amplicon were used as template to be combined by overlap extension PCR with primers DENV-E_BsrGI_For and DENV-E_NheI_Rev. PCR products were separated by agarose gel electrophoresis, purified, and subsequently digested with BsrGI and SphI (both from NEB). The digested insert was cloned into the pDVWSK601 plasmid previously digested with BsrGI and SphI (NEB). The integrity of pDVWSK601 C1218T was verified by full-plasmid sequencing (Microsynth Seqlab). pDVWSK601 C1218T was used to generate pDVWSK601-LucUbi C1218T. The insert was purified from pDVWSK601 C1218T using ScaI (NEB) digestion and ligated with pDVWSK601 LucUbi backbone previously digested with ScaI. The integrity of pDVWSK601-LucUbi C1218T was verified by full-plasmid sequencing (Microsynth Seqlab).

In vitro transcription of DENV gRNA

DENV2 NGC full-length *in vitro* transcripts (IVT) were generated using pDVWSK601, pDVWSK601-LucUbi, and pDVWSK601 C1218T linearized by restriction digestion using XbaI (NEB). Three micrograms of linearized plasmid were incubated at 37°C overnight in a transcription reaction containing 140 U T7 RNA polymerase (Promega), rNTP-Mix (containing 3.125 mM ATP, CTP, and UTP and 1.56 mM GTP; all from Roche), 100 U RNasin ribonuclease inhibitor (Promega), and 1 mM m^{7}G(5′)ppp(5′)G RNA cap analogue (NEB) in 1× RRL buffer (80 mM HEPES-KOH pH 7.5, 12 mM $MgCl_2$, 2 mM spermidine, 40 mM DTT in HPLC water). RNA was extracted using 0.3 M sodium acetate pH 4.5 and acid phenol:chloroform:isoamyl alcohol pH 4.5 (Ambion), followed by isopropanol precipitation and resuspension in nuclease-free water. RNA integrity was determined by using non-denaturing agarose gel electrophoresis and optical density 260/280 nm ratio.

Virus production and measurement of infectious titers

DENV2 NGC and DENV2 NGC C1218U viral stocks were produced as described previously [28]. In brief, 6 × 10^6 BHK-21 cells were electroporated with 10 μg of DENV gRNA IVT resuspended in Cytomix solution [29] supplemented with 2 mM ATP and 5 mM glutathione. Each electroporation was conducted at 975 μF and 270 V. Cells were then maintained in 10-cm dishes with culture medium supplemented with 15 mM HEPES (Gibco). Virus supernatant was harvested at days 3, 4, 5, and 6 post-electroporation and concentrated with centrifugal filter devices (Centricon plus-70 centrifugal filter, MWCO 100 kDa, Millipore), aliquoted, and stored at −80°C. Viral stock infectious titers were determined by limiting dilution assay and calculation of the 50% tissue culture infective dose ($TCID_{50}$)/ml as previously reported using Huh7 cells [28]. After 72 h of infection, cells were fixed with methanol for 30 min at −20°C. DENV-positive cells were stained using a pan-flavivirus antibody D1-4G2-4-15, produced from the HB112 hybridoma cell line (ATCC) [30].

For DENV2 NGC C1218U viral stocks, RNA was extracted from the supernatant collected daily. Three μg of total RNA were reverse transcribed using the High-Capacity cDNA Reverse Transcription Kit (Applied Biosystems) as recommended by the manufacturer. The region encompassing the C/U substitution was amplified by PCR using the Platinum II Taq Hot-Start DNA Polymerase (Invitrogen) and the following primers: 5′- AGAGAAACCGCGTGTCGACTGTACAACAGCTGACAAAGA G-3′ and 5′-GTGTCATTTCCGACTGCATGCATGCTC TTCCCCTGAGTG-3′. PCR products were purified by gel extraction (Macherey-Nagel) and subjected to Sanger sequencing (Microsynth Seqlab) to ensure that reversion had not occurred during virus amplification.

ViREn: a two-step purification and enrichment method for viral RNAs

Extraction of DENV RNA from infected cells and viral particles

3 × 10^6 Huh7 cells were infected with DENV2 NGC at an MOI of 10 for 48 h. For the purification of DENV gRNA and sfRNA from infected cells, total RNA was extracted using TRIzol reagent as recommended by the manufacturer (Invitrogen). For the purification of DENV gRNA from viral particles, 15 ml of the culture supernatant were concentrated using centrifugal filter devices (Amicon Ultra Centrifugal Filter 100 kDa MWCO, Millipore) before extraction with TRIzol LS reagent as recommended by the manufacturer (Invitrogen). The resulting RNA pellets were subjected to a stepwise enhanced deproteination and purification method. First, the RNA pellets were resuspended in ribosome disassembly buffer [20 mM Tris–HCl, 0.25 mM $MgCl_2$, 150 mM NaCl, 1% Triton X-100, 100 μg/ml cycloheximide, 40 U RNasin ribonuclease inhibitor (Promega), 90 mM ethylenediaminetetraacetic acid (EDTA) pH 8.0 in DEPC-treated H_2O] and tumbled at 4°C for 10 min before extraction with TRIzol LS reagent. Next, the RNA pellets were resuspended in proteinase K buffer (20 mM Tris-Cl pH 7.5, 0.5% SDS, 1 mM EDTA, 40 U RNasin ribonuclease inhibitor, in DEPC H_2O) supplemented with 300 μg/ml proteinase K (Macherey Nagel) and incubated at 42°C for 20 min. Finally, the RNA was extracted using 0.3 M sodium acetate pH 4.5 and acid phenol:chloroform:isoamyl alcohol pH 4.5 (Ambion), followed by isopropanol precipitation. RNA was resuspended in nuclease-free H_2O.

Viral RNA separation by sucrose density gradient ultracentrifugation

Linear sucrose gradients were prepared as follows. Sucrose solutions (790 μl) were layered on top of each other starting with 20% (w/v) sucrose solution at the bottom of the tube (4 ml tubes, Beckman Coulter), 16.25% (w/v), 12.5% (w/v), 8.75% (w/v), and 5% (w/v) sucrose in 1× gradient buffer (50 mM KCl, 10 mM potassium acetate, 0.1 mM EDTA, 200 U/ml of RNasin ribonuclease inhibitor, pH 5.2 in DEPC H_2O). Each sucrose solution layer was frozen at −80°C for 15 min prior to addition of the next layer. Gradient tubes were thawed overnight in a cold room prior to ultracentrifugation. RNA samples were layered on top of the gradient and ultracentrifuged using an SW60TI rotor (Beckman Coulter) at 43 800 rpm for 4 h at 4°C. Following centrifugation, gradients were manually fractionated from the top (11 fractions,

375 µl each). RNA was extracted from each fraction using 1:1 ratio of extraction buffer (10 mM Tris-HCl pH 7.5, 350 mM NaCl, 10 mM EDTA, 1% SDS, 42% urea in DEPC-treated H_2O). Samples were heated at 65°C for 10 min after addition of 30 µg of GlycoBlue (Invitrogen), 0.3 M sodium acetate pH 4.5, and acid phenol:chloroform:isoamyl alcohol pH 4.5 (Ambion). RNA extraction was followed by isopropanol precipitation.

Full-length DENV gRNA IVT that served as negative control for the detection of RNA modifications by BSSeq and DRS was prepared following the same protocol. In short, 100 µg of DENV gRNA IVT were mixed with total RNA prepared from uninfected Huh7 cells and subjected to sucrose density gradient ultracentrifugation and fractionation as described earlier.

Specific affinity capture of DENV RNAs

RNAs extracted from fractions 3 and 11 were subjected to DENV2 gRNA affinity capture using RNA-seq MagIC beads—dengue virus (DENV2) kit (ElementZero Biolabs), containing a pool of 20 different DNA probes binding across DENV gRNA—following manufacturer instructions. Custom beads were generated for DENV2 sfRNA (ElementZero Bio-Labs). In short, 20 pmol of beads were used to capture either DENV gRNA or sfRNA from 1–3 µg of fractionated total RNA. The captured RNA was eluted in nuclease-free water, and probes were denatured at 92°C.

Quantitative analysis of DENV RNA by RT-qPCR

Probe-based reverse transcription quantitative PCR (RT-qPCR) was employed to quantify DENV RNAs after purification. Briefly, 3 µl of extracted RNA were mixed with 12 µl qPCR mix (qPCRBIO Probe 1-Step Go Lo-ROX, PCR Biosystems) according to the manufacturer instructions and using the following cycling protocol: 50°C 10 min, 95°C 1 min, 95°C 10 s, 60°C 1 min; steps 3–4 were repeated 39 times. Absolute RNA copy numbers of DENV were calculated using a standard curve of purified DENV IVT. DENV RNA (gRNA and sfRNA) and cellular housekeeping transcripts (GAPDH, 18S rRNA, and 28S rRNA) were analyzed in triplicate using a CFX96 Touch Real-Time PCR detection system (Bio-Rad). Specific primers and probes are listed in Table 1. Note that a DENV 3′UTR probe was employed for the detection of both DENV2 NGC gRNA and sfRNA and a DENV E probe to detect specifically DENV2 NGC gRNA.

Sedimentation analysis of DENV RNA by northern blot analysis

RNA from each sucrose fraction was loaded and separated by electrophoresis on a 1% agarose denaturing gel. RNA was then transferred by capillarity overnight to a positively charged nylon membrane (Roche) using 20× SSC buffer (3 M NaCl, 0.3 M sodium citrate, pH 7.0 in DEPC-treated H_2O). DENV-specific probes, targeting NS1-encoding or 3′UTR regions, were generated freshly using the above-described IVT protocol and DIG-labeled rNTP (Roche) (Table 2). DENV RNA was detected using DIG northern reagents (Roche), following manufacturer instructions. Signals on northern blot membranes were imaged using an ECL Chemocam Imager (Intas Science Imaging Instruments). Bands were quantified using the LabImage 1D Software (Intas Science Imaging).

Estimation of DENV RNA enrichment after affinity capture by RNA-seq

Sequencing libraries were produced with the NEBNext Ultra II Directional RNA Library Prep Kit and sequenced on a NextSeq550 System (Illumina). The 80 nt long single-end reads were first aligned to human rRNA sequences as downloaded from the UCSC Genome Browser using bowtie v1.2.2 [31]. Reads that did not align to rRNA were further aligned to the human genome (hg38) using STAR v2.5.4b [32], providing a gtf file with the exonic coordinates of the basic set of Gencode V38. Read counts were summarized at the gene level using featureCounts [33], only counting reads that are fully contained within exonic regions. Finally, reads that did not align to human genomic sequences were aligned to the DENV2 NGC full plasmid sequence with Bowtie. In all alignment steps, up to two mismatches were allowed. Read coverages on the DENV2 sequence were visualized with Integrative Genomics Viewer (IGV) [34].

Illumina-based bisulfite sequencing

Two hundred nanograms of DENV gRNA from Huh7 cells or 200 ng DENV full-length IVT were used for bisulfite conversion according to Dai and colleagues [35]. After bisulfite conversion and desulphonation, RNAs were first end-repaired and purified before being converted to libraries using NEBNext small RNA library kit (NEB). The DNA libraries were quantified using a fluorometer (Qubit 3.0 fluorometer, Invitrogen) and qualified using Agilent TapeStation 4150. Libraries were multiplexed and subjected to high-throughput sequencing on an Illumina NextSeq2000 instrument with a 75 bp single-end read mode.

Targeted MiSeq bisulfite sequencing

One microgram of RNA extracted from fraction 11 or from total RNA was used for bisulfite conversion using the EZ RNA Methylation Kit (Zymo Research). RNA was reverse transcribed to cDNA using High-Capacity cDNA Reverse Transcription Kit as recommended by the manufacturer (Applied Biosystems). The DENV gRNA targeted region (nt 1106–1266), encompassing the CUCCA motif, was amplified by PCR using the Platinum II Taq Hot-Start DNA Polymerase (Invitrogen) using the following primers: forward: 5′-GGAAGTATTGTATAGAGGTAAAG-3′ and reverse: 5′-CCAAATAATCCACATCCATTTCCCC-3′. PCR products were purified by gel extraction (Macherey-Nagel) and subjected to MiSeq (Illumina) or to Sanger sequencing (Microsynth Seqlab). Individual PCR products were barcoded using Nextera XT Index Kit v2 Set A and subjected to MiSeq using MiSeq Reagent Nano Kit v2 (300 cycles; Illumina). The occurrence of m^5C modifications was analyzed and visualized using the web-based pipeline BisAMP (https://bisamp.dkfz.de/index.php?site=4) [36].

Nanopore DRS of DENV gRNA and IVT

Complementary DNA oligos were designed to dissolve DENV gRNA secondary structures by tiling along the RNA [37]. In total, 100 oligos (Supplementary Table S1) were dissolved at 100 µM and mixed equimolarly. For DRS, the oligo mix was diluted 1:10.

One microliter of oligo mix was combined with 8 µl purified, polyadenylated DENV gRNA or IVT and 1 µl 10× hy-

Table 1. List of primers and probes used for qRT-PCR

Primer Pair/Probe	Sequences
DENV 3′UTR fw	5′ - GGAAAGACCAGAGATCCTGCTGT -3′
DENV 3′UTR rev	5′ - CATTCCATTTTCTGGCGTTC -3′
DENV 3′UTR probe	5′ - 6-FAM – CAGCATCATTCCAGGCACAG - BHQ1 - 3′
DENV E fw	5′ - CAGGTTATGGCACTGTCACGAT -3′
DENV E rev	5′ - CCATCTGCAGCAACACCATCTC -3′
DENV E probe	5′ - 6-FAM – CTCTCCGAGAACAGGCCTCGACTTCAA - BHQ1 - 3′
18S rRNA fw	5′ - GTTGGTGGAGCGATTTGTCTG -3′
18S rRNA rev	5′ - AGGGCAGGGACTTAATCAACG -3′
18S rRNA probe	5′ - VIC - GATGGGGATCGGGGATTGCAATTAT - TAMRA -3′
28S rRNA fw	5′ - AGTCGGGTTGCTTGGGAATGC -3′
28S rRNA rev	5′ - CCCTTACGGTACTTGTTGACT -3′
28S rRNA probe	5′ - Cy5 - TAAGGTAGCCAAATGCCTCG - QSY2 -3′
GAPDH fw	5′ - GAAGGTGAAGGTCGGAGTC -3′
GAPDH rev	5′ - GAAGATGGTGATGGGATTTC -3′
GAPDH probe	5′ - VIC - CAAGCTTCCCGTTCTCAGCCT - TAMRA -3′

Table 2. Sequences of DIG-labeled probes used for northern blot

DIG-DENV NS1 probe (nt 2460–2796)	5′-GAAGUGUGGCAGUGGGAUUUUCAUCACAGACAACGUGCACACAUGGACAGAACAAU ACAAGUUCCAACCAGAAUCCCCUUCAAAGCUAGCUUCAGCUAUCCAGAAAGCUCAUGA AGAGGGCAUUUGUGGAAUCCGCUCAGUAACAAGACUGGAAAAUCUGAUGUGGAAACAA AUAACACCAGAAUUGAAUCACAUUCUAUCAGAAAAUGAGGUGAAGUUGACUAUUAUGAC AGGAGACAUCAAAGGAAUCAUGCAGGCAGGAAAACGAUCUCUGCAGCCCCAGCCCACU GAGCUGAAGUAUUCAUGGAAAACAUGGGGCAAAGCGAAAAUGCUCUCU-3′
DIG-DENV 3’UTR probe (nt 10 312–10 593)	5′-GGAUUAAGCCAUAGUACGGAAAAAACUAUGCUACCUGUGAGCCCCGUCCAAGGACGU UAAAAGAAGUCAGGCCAUUACAAAUGCCAUAGCUUGAGUAAACUGUGCAGCCUGUAGCU CCACCUGAGAAGGUGUAAAAAAUCUGGGAGGCCACAAACCAUGGAAGCUGUACGCAUGG CGUAGUGGACUAGCGGUUAGAGGAGACCCCUCCCUUACAAAUCGCAGCAACAAUGGGGG CCCAAGGUGAGAUGAAGCUGUAGUCUCACUGGAAGGACUAGAGGUUAG-3′

bridization buffer (f.c. 10 mM Tris pH 7.5, 50 mM NaCl). In a PCR thermocycler, the DENV gRNA was first denatured (5 min, 95°C) and then annealed to the oligos by slowly decreasing the temperature (0.1°C/s to 22°C). The oligo-annealed DENV gRNA was immediately subjected to DRS library preparation with SQK-RNA004 (ONT) by addition of 3 μl 5 × Quick ligation buffer (NEB), 1 μl RTA (ONT), and 1 μl T4 DNA ligase, high concentration (NEB). Adapter ligation was carried out for 10 min at room temperature. To resolve remaining secondary structures, a complementary DNA strand was synthesized with Induro Reverse Transcriptase (RT, NEB). To 15 μl ligation, 14 μl H_2O, 8 μl 5× Induro RT reaction buffer, 2 μl 10 mM dNTPs (Thermo Fisher Scientific), and 1 μl Induro RT were added and incubated 30 min at 60°C, followed by 10 min denaturation at 70°C. Reactions were cleaned up with 1.8× RNA Clean XP beads (Beckman Coulter), washed two times with 80% ethanol, and eluted in 13 μl H_2O. In a total volume of 20 μl, the RLA adapter (ONT) was ligated as described earlier. Reactions were cleaned up with 1× RNA Clean XP beads, washed two times with ONT wash buffer, and eluted in 33 μl REB (ONT). The concentration of the library was determined with the Qubit dsDNA HS kit (Thermo Fisher Scientific). Libraries were loaded on RP4 Promethion flow cells as described in the manufacturer's protocol. Sequencing was performed overnight on a P24. A series device equipped with MinKNOW v24.06.14. POD5 files were called with Dorado v0.8.2 and the rna004_130bps_sup@v5.1.0 model and the modified bases option ("–modified-bases m5C inosine_m6A pseU") enabled. Data were aligned with minimap2 v2.28 and modkit v0.4.2 (ONT) was used to generate the corresponding bedmethyl files (modification threshold = 0.95, Supplementary Table S2).

Preparation of oligonucleotides for accurate m^{5}C Nanopore reads basecalling

RNA oligonucleotide phosphorylation and ligation

Sequencing reads from m^{5}C-modified and unmodified oligonucleotides were generated to train ONT's Dorado basecaller. Unmodified 5′ and 3′ oligonucleotides were purchased from biomers.net. The central m^{5}C-modified oligonucleotide was purchased from Dharmacon (see Table 3). An equimolar mixture of the three RNA oligonucleotides (with modified or unmodified central oligonucleotide) was phosphorylated at the 5′ end using 0.75 U/μl T4 polynucleotide kinase (Thermo Fisher Scientific) per 30 μM of RNA in 1× kinase-ligase buffer (50 mM Tris-Cl pH 7.4, 10 mM $MgCl_2$, 5 mM DTT, 2 mM ATP) for 60 min at 37°C. The phosphorylated oligonucleotides were immediately used for ligation by adding 2% less complementary DNA splint to the reaction mixture. For this experiment, RNA oligonucleotides of 900 pmol each were hybridized to 882 pmol of DNA splint by heating at 75°C for 4 min, followed by slow cooling to room temperature over 15 min.

Ligation was initiated by adding 2 U/μl T4 DNA Ligase (Thermo Fisher Scientific), and the reaction was incubated overnight at 16°C. To remove the DNA splint, DNase I (Thermo Fisher Scientific) was added at a final concentration of 0.1 U/μl, followed by incubation at 37°C for 30 min. The ligated construct was purified from unligated oligonucleotides

Table 3. Sequences of RNA oligonucleotides used for ligation

Oligonucleotide	Sequence
Oligo1	5′-GAACCCAGCCUAAAUGAAGAGCAGGACAAAAGGUUCGUC-3′
Oligo2 unmodified	5′-GCAAACACUCCAUGGUGGA-3′
Oligo2 modified	5′-GCAAACA[m^{5}C]UCCAUGGUGGA-3′
Oligo3	5′-CAGAGGAUGGGGAAAUGGAUGUGGAUUAUUUGGAAAAGGA-3′

using an 8% denaturing polyacrylamide gel and electrophoresis. RNA purity and concentration were assessed using a NanoDrop 2000 (Thermo Fisher Scientific).

Polyadenylation and DRS library preparation

The ligated RNA m^{5}C-modified and unmodified oligonucleotides were polyadenylated at the 3′ end using *Escherichia coli* poly(A) polymerase (NEB) according to the manufacturer protocol. The RNA was then purified using the Oligo Clean & Concentrator Kit (Zymo Research) before proceeding to library preparation. Library preparation was performed using 1 μg of polyadenylated RNA with the SQK-RNA004 kit (ONT), following the manufacturer's standardized protocol. In this step, SuperScript III Reverse Transcriptase (Invitrogen) was used instead of Induro Reverse Transcriptase (New England Biolabs). The prepared libraries were quantified using the Qubit dsDNA HS Assay Kit (Invitrogen), loaded onto MinION flow cells, and sequenced with MinKNOW (version 24.02.26) for 72 h.

Analysis of NSUN6 expression during DENV infection by western blot analysis

Huh7 cells (1×10^5 cells/well) were seeded into a six-well plate one day before infection with DENV2 NGC at an MOI of 10 or mock treatment. Medium was replaced 6 h after the addition of the virus and cells were harvested at the indicated time points after virus addition. Cells were washed with PBS and collected by scraping into ice-cold protein lysis buffer [50 mM Tris–HCl pH 7.4, 150 mM NaCl, 1% Triton X-100, supplemented with 60 mM β-glycerophosphate, 15 mM 4-nitrophenylphosphate, 1 mM sodium orthovanadate, 1 mM sodium fluoride, and EDTA-free cOmplete protease inhibitor cocktail (Roche)]. Cells were lysed for 30 min on ice followed by centrifugation for 15 min at 16 000 × *g* at 4°C. Total protein concentration of clarified lysate was determined by the Bradford method using Protein Assay Dye Reagent (Bio-Rad) and absorbance measurement at 595 nm.

Equal amounts of total protein (20 μg) were denatured for 5 min at 95°C in reducing 1× Laemmli buffer (62.5 mM Tris–HCl pH 6.8, 8.33% glycerol, 1.5% SDS, 1.5% β-mercaptoethanol, 0.005% bromophenol blue) and separated on a 10% resolving gel by sodium dodecyl sulfate–polyacrylamide gel electrophoresis (SDS–PAGE) in buffer containing 25 mM Tris–HCl pH 8.8, 192 mM glycine, and 0.1% (w/v) SDS. Proteins were transferred to a 0.45 μm polyvinylidene difluoride membrane (Millipore) by tank blotting at 360 mA for 2.5 h at 4°C in transfer buffer [25 mM Tris–HCl pH 8.3, 150 mM glycine, and 20% (v/v) methanol]. Membranes were blocked with 5% (w/v) powdered milk (Roth) in Tris-buffered saline containing 0.1% Tween 20 (50 mM Tris–HCl pH 7.4, 150 mM NaCl, 0.1% Tween 20) for 1 h. Immunostaining was performed in blocking buffer by incubating membrane sections overnight at 4°C with rabbit polyclonal anti-NSUN6 (GeneTex, 1:1000), mouse monoclonal anti-GAPDH (Santa Cruz Biotechnology, 1:5000), or rabbit polyclonal anti-DENV NS5 (GeneTex, 1:1000), followed by incubation for 2 h with goat polyclonal secondary antibodies conjugated to horseradish peroxidase (all from Sigma–Aldrich). Proteins were detected by chemiluminescence using Western Lightning Plus enhanced chemiluminescence (ECL) reagent (Perkin Elmer) and detection on an ECL Chemocam Imager (Intas Science Imaging). Band intensities were quantified using Image Studio Lite software (Li-Cor, version 5.2.2). The statistical comparison between DENV-infected and mock samples were performed using two-way ANOVA with multiple comparisons (GraphPad Prism v8.4.3).

Generation of Huh7 NSUN6 knockout cell clones by CRISPR/Cas9 approach

Huh7 knockout (KO) cell clones were generated using a two-CRISPR RNA (crRNA) approach as described in [38]. Two crRNAs targeting the NSUN6 locus at exons 1 and 3 (5′-/AltR1/GCATTTCTCTTGGTGGAGAAC/AltR2/-3′, 5′-/AltR1/CATGACAGAGTCTAAAGTCTGC/AltR2/-3′) were purchased from IDT. In brief, non-targeting (NT) control cell lines were generated with the CRISPR–Cas9 negative control crRNA#1 (IDT). Individual crRNAs and tracrRNA (IDT) were resuspended in TE buffer (10 mM Tris, 0.1 mM EDTA, pH 7.5) to a final concentration of 200 μM and hybridized at equimolar amounts by heating to 95°C for 5 min and slow stepwise cooling to room temperature. Pre-assembled crRNA/Cas9 ribonucleoprotein complexes (RNPs) were obtained by gently mixing 1.2 μl of hybridized RNAs with 17 μg of recombinant Cas9 protein (IDT) and 2.1 μl of PBS, followed by 20 min incubation at room temperature.

2×10^6 Huh7 cells were resuspended in 91 μl supplemented Solution T (Lonza) and mixed with 2.5 μl of each pre-assembled RNP and 4 μl electroporation enhancer (IDT). Nucleofection was performed using an Amaxa 2b nucleofector (Lonza) and pre-set program T-22. Nucleofected cells were mixed with pre-warmed conditioned medium and seeded. After 48 h cells were seeded for clonal amplification in 96-well plates. Homozygous clones were screened using target-specific PCR (Platinum II Taq hot-start DNA polymerase, Invitrogen) on genomic DNA using the following primers: NSUN6-KO-For: 5′– TCGGCTAGGCTTGAGAAA GC –3′ and NSUN6-KO-Rev: 5′– AGGGTTTCGCCATACTGG –3′. The expression of NSUN6 in homozygous cell clones was further analyzed by immunoblotting.

For further analysis, Huh7 cell pools were prepared to account for single-cell clone variation. Equal numbers of Huh7 NT cell clones (#1, 2, 3, 4, and 8) and Huh7 NSUN6 KO cell clones (#1, 19, 29, and 33) were mixed and frozen. Cell pools were thawed and used for experiments within 5 passages.

Characterization of NSUN6 KO cell clones

Analysis of cell growth

Cell growth was measured using IncuCyte live-cell analysis system (Sartorius). 3×10^3 cells per well were seeded in a 96-well plate. Cells were incubated at 37°C overnight before starting the live-cell analysis for 5 days. Specifically, cell growth was measured by imaging 4 fields of view for each well at 3-h intervals. Cells were counted, and growth curves were generated using the IncuCyte live-cell analysis system. Values were normalized to T_0. Statistical analysis was performed using two-way ANOVA (GraphPad Prism v8.4.3).

Measurement of global translation by flow cytometry

The global translation level of Huh7 NT and NSUN6 KO cells was measured by assessing the incorporation of fluorescently labeled puromycin using the Click-iT Plus OPP Alexa Fluor 488 Protein Synthesis Assay Kit (Invitrogen) and flow cytometry (Becton Dickinson FACSCelesta Cell Analyzer). In brief, 2×10^5 cells were seeded in triplicate in six-well plates the day before measurements. Huh7 NT cells treated with 200 μg/ml cycloheximide for 1 h were used as negative control (repressed global translation). Cells were treated with 50 μM OP-puro for 1 h at 37°C before fixation with 4% paraformaldehyde (PFA) in PBS for 15 min on ice (in the dark). Cells were washed once with 2 ml PBS before membrane permeabilization with 1 ml 3% FBS and 0.1% saponin in PBS for 5 min. Cells were resuspended in Click-iT reaction buffer as recommended by the manufacturer and washed twice with PBS supplemented with 3% FBS and 0.1% saponin before analysis by flow cytometry. Statistical analysis of the technical replicates was performed using unpaired t-test (GraphPad Prism v8.4.3).

LC-MS/MS analysis of tRNA^{Thr} m^{5}C levels in Huh7 NSUN6 KO cells

Purification of tRNA^{Thr} was based on a method by Kristen and colleagues [39]. In detail, 6 μg of purified total tRNAs from either Huh7 NT or NSUN6 KO cells were mixed with 30 pmol of each FAM-labeled cDOQ (see Table 4) (all purchased from IDT) in a hybridization buffer (30 mM HEPES pH 7.5, 100 mM potassium acetate). Hybridization was performed by incubating at 95°C for 1 min, followed by a stepwise reduction (5°C/30 s) down to 70°C, followed by 5°C/min to 30°C, and 2.5°C/min to 20°C. Samples were loaded on a 10% native polyacrylamide gel prepared according to supplier's protocol (Carl Roth). Gel was run for 1:30 h at 45 mA followed by visualization using a Typhoon Trio+ (ex: 488 nm, em: 520 nm BP, Amersham Biosciences). Shifted bands were cut with a scalpel, smashed, and resuspended in 500 μl of 500 mM ammonium acetate (Carl Roth). Gel pieces were frozen at −80°C, then incubated at 15°C overnight under slight shaking. The next day, solutions were filtered using 0.45 μm Nanoseps (PALL) and precipitated using 1 μl GlycoBlue (Invitrogen) and 1 ml ethanol. Afterward, DNA oligonucleotides were digested using 2 U DNase I-XT (NEB) in its respective reaction buffer for 1 h at 37°C. Finally, samples were purified using RNA Clean & Concentrator-5 (Zymo Research) and eluted in 6 μl nuclease-free water.

Two hundred nanograms of tRNA^{Thr} purified from Huh7 NT or NUSUN6 KO cells were digested with 0.2 U snake venom phosphodiesterase from *C. adamanteus* (Worthington), 10 U benzonase (Sigma–Aldrich), 0.2 U bovine intestine phosphatase (Sigma–Aldrich), 0.6 U nuclease P1 from *P. citrinum* (Sigma–Aldrich), and 200 ng pentostatin (Sigma–Aldrich) in a total volume of 20 μl buffer (5 mM Tris pH 8, 1 mM $MgCl_2$). Reaction was incubated for 2 h at 37°C and stopped by addition of 30 μl nuclease-free water. The LC-MS/MS device was an Agilent 1260 Infinity (II) with an Agilent 6460A triple quadrupole mass spectrometer equipped with an electrospray ion source with following parameters: gas temperature 350°C, gas flow 8 l/min, nebulizer pressure 50 psi, sheath gas temperature 350°C, sheath gas flow 12 l/min, capillary voltage 3000 V, and nozzle voltage 0 V. A Synergi 4 μm Fusion-RP 80 Å 250 × 2 mm (Phenomenex) was used as column. Separation was achieved using a two-component gradient with solvent A [5 mM ammonium acetate pH 5.3 (Sigma–Aldrich), adjusted with acetic acid, supplemented with 1% (v/v) acetonitrile (Honeywell)] and solvent B [acetonitrile with 1% (v/v) nuclease-free water]. The gradient started with 100% solvent A, followed by a linear increase to 8% solvent B within 10 min. Solvent B was further increased to 40% within another 10 min to finally decrease to 100% solvent A in 3 min. Subsequent equilibration was performed for 7 min. Flow rate was constant at 0.35 ml/min. Canonical nucleosides were detected using a diode array detector at 254 nm while modified nucleosides were detected using dynamic multiple reaction monitoring (dMRM) in positive mode with following parameters: m^{5}C mass transition: 258 → 126.1, retention time: 7.9 min; m^{3}C mass transition: 258 → 126, retention time: 4.4 min. Quantification was performed as previously described [40]. In short, external calibration was performed by measuring increasing amounts of modified nucleoside standards (1 to 5000 fmol) or canonical nucleoside standards (0.5 to 500 pmol). Internal calibration was performed by addition of ^{13}C-labeled internal standard from ^{13}C-fed yeast. The respective slopes of the calibration curves were used to calculate the amounts. Modified nucleosides were set in relation to the detected adenosine amount of the respective sample. Results were set in relation to Huh7 NT.

Measurement of viral replication

Replication of DENV2 NGC WT and C1218U firefly luciferase reporter viruses was measured as previously described [28]. Five micrograms of DENV full-length firefly reporter IVT were electroporated into 1×10^6 Huh7 parental, NT, or NSUN6 KO cells suspended in Cytomix solution supplemented with 2 mM ATP and 5 mM glutathione. Electroporation was conducted at 500 μF and 166 V. For the time points 4 h and 24 h post-electroporation, 1.1×10^5 cells were seeded in duplicates in a 24-well plate. For the time points 48 h, 72 h, and 96 h, 6.5×10^4 cells were seeded in duplicates in a 24-well plate. Half of the cells were co-treated with 27 μM NITD008 (Tocris Bioscience) to inhibit DENV RNA-dependent RNA polymerase NS5 activity and viral RNA synthesis [41]. DMSO was used as vehicle control. Cells were harvested at the indicated time points by addition of luciferase lysis buffer (25 mM Gly–Gly pH 7.8, 15 mM $MgSO_4$, 15 mM K_3PO_4, 4 mM EGTA, 10% glycerol, 0.1% Triton X-100 supplemented with 1 mM DTT) and immediately stored at −80°C. For measurements of the firefly luciferase activity, 100 μl cell lysates were mixed with 100 μl assay buffer (25 mM Gly–Gly pH 7.8, 15 mM $MgSO_4$, 15 mM K_3PO_4, 4 mM EGTA) supplemented with 1 mM DTT, 2 mM ATP, and 70 μM D-luciferin (P.J.K). All measurements were done in duplicates using a tube luminometer (Berthold Technologies). Replication efficiency was

Table 4. Sequences of oligonucleotides used for DORQ-seq

Oligonucleotide	Sequence
cDOQ Thr 1	5′-FAM-AGACGTGTGCTCTTCCGATCTTGGAGGCCCCGCTGGGATTCGAACCCAGGATCTC CTGTTTGATCGTCGGACTGTAGAACTCTGAAC-3′
cDOQ Thr 2	5′-FAM-AGACGTGTGCTCTTCCGATCTTGGAGGCACGGACGGGGTTCGAACCCGTGATCTT CGGTTTGATCGTCGGACTGTAGAACTCTGAAC-3′
cDOQ Thr 3	5′-FAM-AGACGTGTGCTCTTCCGATCTTGGAGGCCCCAGCGAGATTTGAACTCGCGACCC CTGGTTTGATCGTCGGACTGTAGAACTCTGAAC-3′

determined by normalization to the 4-h values, which reflects transfection efficiency. Statistical analysis was performed using two-way ANOVA (GraphPad Prism v8.4.3).

NSUN6 *in vitro* methylation assay

Bacterial expression and purification of human full-length NSUN6

Plasmid used for overexpression is available at Addgene (ID#188060). Transformed *E. coli* Rosetta (DE3) pLysS cells were grown in terrific broth medium at 37°C until optical density at 600 nm wavelength reached 0.7. After precooling to 16°C, overexpression was induced by 500 μM isopropyl-β-D-thiogalactopyranoside (IPTG) for 18–20 h. Cell pellets were flash frozen in liquid nitrogen and stored at −80°C. Cell pellets were disrupted in lysis buffer (50 mM sodium phosphate pH 7.5, 150 mM NaCl, 10 mM imidazole, 0.1% polysorbate-20). Ni affinity chromatography was performed with HisTrap HP 5 ml (Cytiva) column. Protein was eluted with the elution buffer (50 mM sodium phosphate pH 7.5, 150 mM NaCl, 500 mM imidazole, 0.1% polysorbate-20) and was further purified with size exclusion chromatography on the Superdex 16/600 75 pg column (Cytiva), equilibrated with SEC buffer (25 mM HEPES pH 7.5, 300 mM NaCl, 1 mM DTT, 0.1% polysorbate-20, 10% glycerol). NSUN6 protein was concentrated with the help of Amicon Ultra Centrifugal Filter (10 kDa, MWCO, Millipore), then aliquoted, flash frozen with liquid nitrogen, and kept at −80°C until further use. The purity and quantity of the recombinant proteins were assessed by SDS–PAGE followed by staining with Coomassie blue.

Tritium incorporation assay for NSUN6

RNA methylation was carried out in triplicate for 60 min in the reaction buffer (50 mM Tris–HCl pH 7.0, 50 mM NaCl, 5 mM $MgCl_2$, 1 mM DTT, 5% DMSO). Recombinant NSUN6 was added at the final concentration of 30 nM, together with the methyl group donor S-adenosyl-L-methionine (SAM). A mixture of cold SAM (NEB) and ^{3}H-SAM (Hartmann Analytics) was added to the final concentrations of 1.2 μM and 0.038 μCi μl^{-1}. Different DENV RNA substrates were added to the same molar concentration of 750 nM. The $tRNA^{Thr}$, a known NSUN6 substrate, was used as a positive control at the same molar concentration and refolded by 5 min incubation at 75°C. An IVT of the eGFP-coding sequence, containing no CUCCA motifs, was used as negative control. Eight microliters of solutions were spotted onto the filters (Whatman) and placed into the ice-cold 5% trichloroacetic acid (TCA) (Sigma–Aldrich) for RNA precipitation and incubated for at least 15 min. All other washing steps were performed at room temperature, namely two more in TCA for 20 and 10 min, and the last one in ethanol for 10 min. Washed filters were dried in the fume hood overnight or under the infrared lamp for 40–60 min. Dry filters were transferred into scintillation vials with 3 ml of Ultima Gold liquid scintillation cocktail (Sigma–Aldrich). The relative amount of ^{3}H-methyl groups transferred onto RNA was measured as counts per minute (CPM) with the Tri-Carb 2810TR Low Activity Liquid Scintillation Analyzer (Perkin Elmer). Statistical analysis of the technical replicates was performed using unpaired t-test (GraphPad Prism v8.4.3).

Impact of m^5C modification on DENV gRNA turnover and virus production

Measurement of gRNA turnover

2.8×10^5 cells (Huh7 NT cells, Huh7 NSUN6 KO, or Huh7 parental cells) were seeded per well in six-well plates the day before infection. Cells were infected with DENV2 NGC WT or DENV2 C12181U at an MOI of 0.1. Twenty-four hours post infection, cells were treated with 27 μM NITD008 (Tocris Bioscience) to inhibit viral RNA synthesis and with DMSO as a vehicle control. Cells were harvested at 24-h intervals for up to 5 days after treatment with NITD008. Total RNA was extracted with TRIzol reagent (Invitrogen) as recommended by the manufacturer. DENV gRNA copies were quantified by probe-based qRT-PCR as described earlier. DENV gRNA levels were normalized to that of *GAPDH* mRNA. Fold changes in abundance relative to time point 24 h were calculated using the ΔΔCT method [42] and expressed as a percentage. The resulting decay curves were obtained by using a non-linear regression (GraphPad Prism) to estimate the mRNA half-life ($t_{1/2}$). For half-lives exceeding 100 h or which could not be determined, values are indicated as ">100 h". Statistical comparison of the decay curves was performed using two-way ANOVA (GraphPad Prism v8.4.3).

Measurement of intracellular and extracellular infectious titers

To measure the impact of gRNA accumulation in Huh7 cells infected with DENV2 NGC WT or DENV2 C12181U, particles were harvested at 24 h (for normalization) and 72 h. For extracellular particles (released in the supernatant), supernatants were supplemented with 15 mM HEPES and filtered through 0.45 μm pore-sized membranes to remove cellular debris. To harvest intracellular particles (assembled viral particles to be released), cells were washed twice with 1× PBS, scraped in 1 ml medium supplemented with 15 mM HEPES, and subjected to three successive freeze-thaw cycles. Cell debris were removed by centrifugation at 20 000 × *g* for 10 min at 4°C. Both intracellular and extracellular virus titers were determined by serial limiting dilution as described above. All values were normalized to time point 24 h. The statistical comparison of the infectious titer at 72 h was performed us-

ing two-way ANOVA with multiple comparisons (GraphPad Prism v8.4.3).

Cell viability assay

5×10^3 cells per well were seeded in triplicate for each sample in a 96-well plate the day before infection. Cells were infected by DENV2 NGC or DENV2 C12181U at an MOI of 0.1. Cell viability was measured in triplicate wells at 24-h intervals for up to 5 days using the Cell Proliferation Reagent WST-1 (Roche) following manufacturer's instructions. In short, cells were incubated with WST-1 reagent pre-diluted 1:10 in medium for 30 min at 37°C before addition of Triton X-100 to a final concentration of 1%. Triplicate wells containing medium only served as control for background signals. The formation of formazan was quantified by measuring absorbance at 450 nm (and a 620 nm reference filter) using a microplate reader (Tecan). The average absorbance of blank wells containing only culture medium and WST-1 reagent (background control) was subtracted from the average value of each sample. All values were normalized to time point 24 h. The statistical comparison of the cell viability curves was performed using two-way ANOVA (GraphPad Prism v8.4.3).

Results

ViREn: a two-step method to purify and enrich DENV RNA

Enrichment and purity of target RNA are crucial for enhancing sequencing coverage and enabling RNA modification mapping, particularly for low-abundance RNAs. We set out to develop a two-step viral RNA purification and enrichment approach—called ViREn—for the isolation of DENV RNA from infected cells and virions (Fig. 1A). This method is based on the sedimentation coefficient of viral RNAs in sucrose density gradients. Early studies showed the presence of two DENV RNA species in infected cells, which separated into distinct fractions during gradient ultracentrifugation: a 40–45S species corresponding to gRNA and a 6–8S species, whose origin was unknown at the time, likely corresponding to sfRNA [43, 44].

We first extracted total RNA from Huh7 cells infected with DENV for 48 h. To increase the recovery rate of viral RNA, especially of gRNA associated with translating ribosomes, total RNA was treated with EDTA to disrupt polysomes and extensively deproteinized using proteinase K (Supplementary Fig. S1A and B). Next, the RNA was separated on a 5%–20% sucrose density gradient by ultracentrifugation (Fig. 1A). The separation of tRNAs and rRNAs after fractionation and RNA extraction was confirmed by gel electrophoresis (Fig. 1B). The distribution of DENV gRNA and sfRNA across the gradient was analyzed by northern blot analysis using a probe specific for DENV 3′UTR. Consistent with previous reports, the majority of DENV gRNA sedimented in the fraction with the highest sucrose density (fraction 11), separating it from most cellular RNAs (Fig. 1B). A second band was detected in all gradient fractions, with highest abundance in fraction 3 (Fig. 1B and Supplementary Fig. S1C). This band corresponded to DENV sfRNA, as confirmed by the absence of the signal when using a hybridization probe targeting the NS1-coding sequence at the 5′ end of DENV gRNA (Supplementary Fig. S1C). Next, sucrose density ultracentrifugation was also applied to purify gRNA from viral particles in culture supernatant. As anticipated, most of the gRNA sedimented in fraction 11 (Fig. 1C). Importantly, for both cell- and virion-derived gRNAs, the gradient separated intermediate-sized viral RNA, likely degradation products or synthesis intermediates, which may be released into the culture medium as a result of virus-induced cell death, thus providing an effective first step for enriching intact gRNA.

The second step of ViREn aimed at specifically enriching DENV gRNA and sfRNA by sequence-specific affinity capture to reduce contaminating RNAs that might have co-sedimented. Importantly, this step did not compromise the integrity of the DENV gRNA while further removing intermediate-sized viral RNAs and sfRNA (Fig. 1D). Furthermore, this positive selection effectively reduced rRNAs by almost 5 logs as measured by RT-qPCR (Fig. 1E and Supplementary Fig. S2A). To better assess the performance of ViREn second step, we performed RNA-seq analysis on the RNA extracted from fractions 3 and 11 before and after affinity capture. On average, DENV gRNA was enriched by 15-fold after purification from fraction 11 (Fig. 1F). The sfRNA-specific affinity capture proved to be more efficient with a 28-fold enrichment after capture from fraction 3 (Supplementary Fig. S2B). In agreement with Fig. 1D, analysis of read coverage along the gRNA showed that the additional step of affinity capture removed any remaining sfRNA present in fraction 11, as no read enrichment was detected in the gRNA 3′ end relative to other regions (Supplementary Fig. S2C).

Overall, the ViREn method enabled the efficient enrichment and purification of DENV gRNA and sfRNA, providing a reliable platform for the downstream analysis of RNA modifications at single-base resolution.

Identification of a single m^{5}C-modified site at position 1218 of DENV gRNA

Our study focused on the identification of m^{5}C modifications in DENV gRNA, taking advantage of well-established methods that allow for high-confidence detection and mapping at a single-base resolution [45, 46]. DENV gRNA purified from cells and virions using ViREn was subjected to bisulfite conversion [46, 47] followed by Illumina-based RNA-seq (BSSeq) (Fig. 2A and Supplementary Fig. S3). RNA bisulfite conversion relies on sodium bisulfite selectively deaminating unmodified C to U while leaving m^{5}C intact so that methylated sites can be distinguished after reverse transcription and sequencing. Sources of background noise were reduced by (i) using deamination conditions allowing almost complete conversion of C to U, and (ii) comparative analysis with an unmethylated IVT of the full-length DENV gRNA sequence, which was mixed with total RNA from uninfected cells and subjected to ViREn. Analysis was performed in three biological replicates. Stringent analysis of the cytosine pattern revealed a prominent m^{5}C site at position 1218 in the envelope protein (E) coding sequence in all three replicates of the gRNA purified from infected cells (Fig. 2A and Supplementary Fig. S3). Strikingly, this modification was not detectable in gRNA purified from virions, suggesting the potential exclusion of m^{5}C-modified gRNAs from packaging into viral particles. The occurrence of m^{5}C at position 1218 was confirmed by targeted MiSeq bisulfite sequencing (Fig. 2B) [36, 46], which established an average methylation level for the three biological replicates of ∼20% (Fig. 2C).

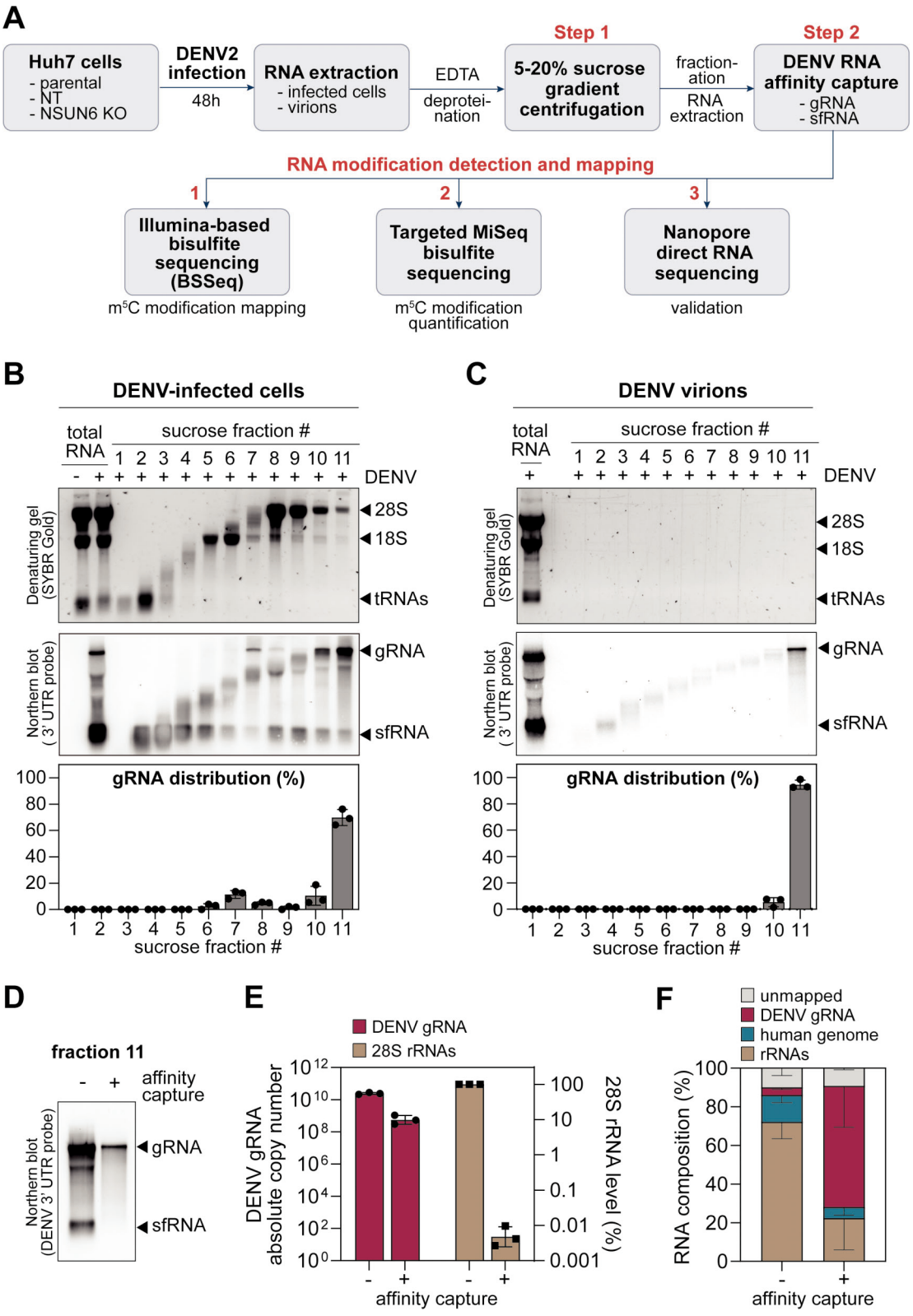

Figure 1. Establishment of ViREn. (**A**) Schematics of the ViREn workflow. DENV RNA from either infected cells or virions was separated by sucrose gradient ultracentrifugation. DENV gRNA and sfRNA were further enriched using antisense affinity capture. The purified DENV gRNA was subjected to RNA sequencing-based approaches for the identification and mapping of m^5C modifications. The distribution of RNAs extracted from infected cells (**B**) and virions (**C**) across sucrose density gradient fractions was analyzed by denaturing agarose gel and corresponding northern blot using a hybridization probe targeting DENV 3′UTR. The percentage of DENV gRNA in each fraction is shown at the bottom (mean ± SD, $n = 3$). (**D**) DENV gRNA collected in fraction 11 was further purified by affinity capture. Its integrity was visualized by northern blotting. (**E**) The level of DENV gRNA and 28S rRNA contaminant, before and after affinity capture, was measured by probe-based RT-qPCR (mean ± SD, $n = 3$). (**F**) The total RNA composition of fraction 11 before and after affinity capture was analyzed by Illumina-based RNA-seq ($n = 3$). Shown is the proportion of reads in each sample corresponding to DENV gRNA, human genome, rRNAs, and unmapped reads (mean ± SD, $n = 3$).

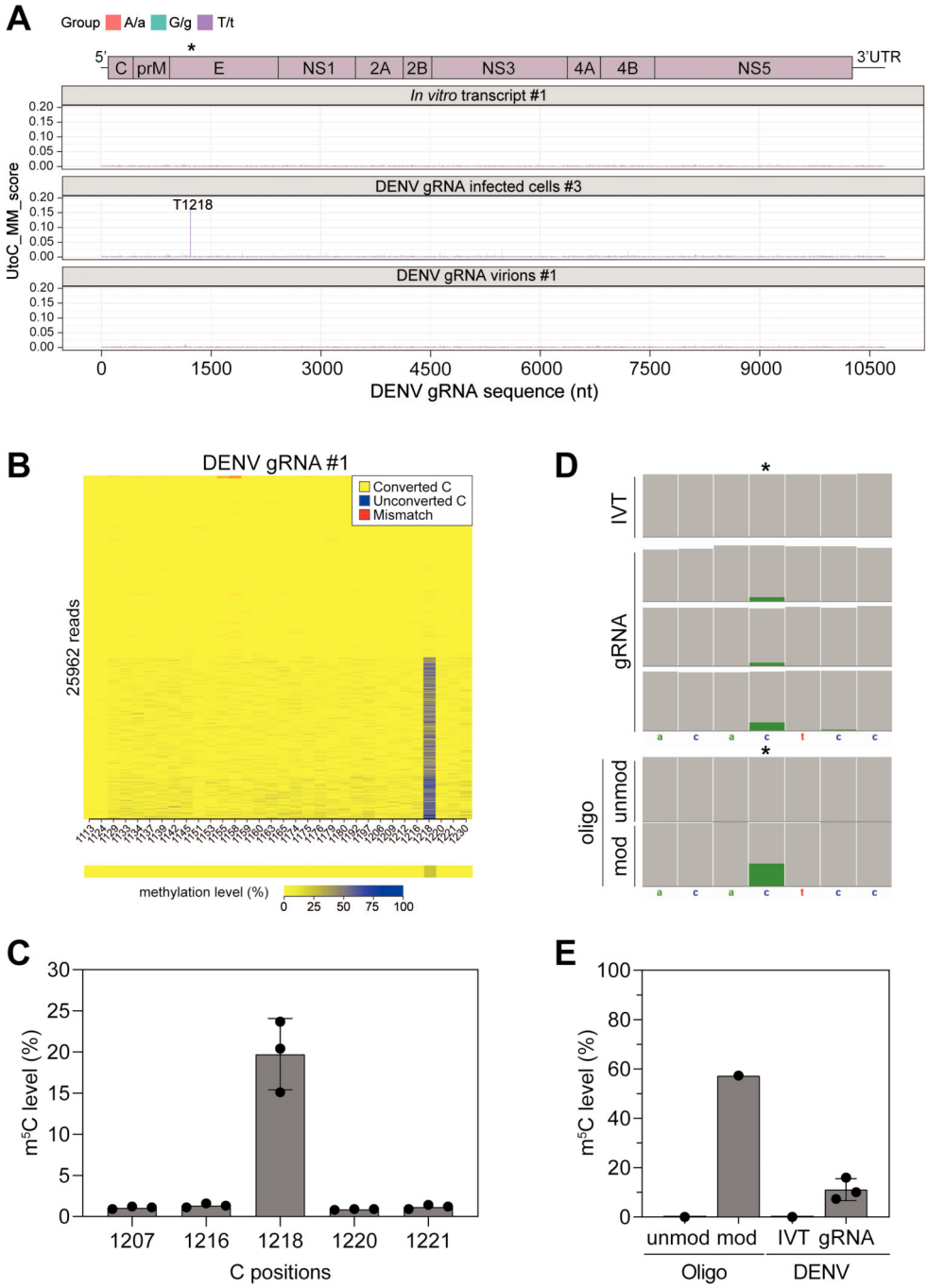

Figure 2. Mapping of m^{5}C on DENV gRNA. (**A**) DENV gRNA purified from infected cells and virions was subjected to BSSeq ($n = 3$). Unmethylated IVT processed with the ViREn method was used for comparative analysis and to reduce background noise. A representation of DENV gRNA is shown on the top. The asterisk marks the m^{5}C position at nt 1218 in the E-coding sequence of DENV gRNA. A schematic of DENV gRNA organization is shown on the top. (**B**, **C**) Analysis of m^{5}C methylation levels in gRNA extracted from infected cells using targeted MiSeq bisulfite sequencing ($n = 3$). Total RNA was extracted and submitted to bisulfite conversion before reverse transcription. An amplicon spanning DENV gRNA nt 1106 to 1266 was amplified by PCR and further processed for MiSeq. (B) The top panel shows a representative methylation heatmap generated using BisAMP [36]. Each row of the heatmap corresponds to a sequencing read. Unconverted (i.e. methylated) cytosines are displayed in blue, while converted (i.e. unmethylated) cytosines are displayed in yellow. Sequencing reads (25 962) are aligned to the reference sequence and ordered from bottom to top according to their overall cytosine methylation level. The bar below the heatmap indicates the corresponding methylation level for each cytosine, expressed as the percentage of reads. This percentage is visualized using a color gradient from yellow (0%, unmethylated) to blue (100%, methylated). (C) Average methylation levels at C1218 and 4 adjacent cytosines (mean ± SD, $n = 3$). (**D**, **E**) Nanopore DRS of DENV gRNA purified from infected cells ($n = 3$). Unmethylated IVT was employed to filter out background noise. Short synthetic oligonucleotides (oligo) either containing an m^{5}C modification at position 1218 (mod) or unmodified (unmod) were sequenced to determine the probability threshold for accurate base-calling using Dorado. (D) Read coverage snapshot of C1218 and adjacent nucleotides was generated with IGV. The coverage gray bars represent absolute read counts aligned at each position. Reads matching the reference sequence are represented in gray. Reads with a modification probability above 0.95 are labeled green. The star indicates the residue C1218. (E) Methylation levels at position 1218 were calculated using the modkit-generated bedmethyl files (Supplementary Table S2), applying a modification probability threshold of 0.95 (mean ± SD, $n = 3$ for DENV gRNA). Note that the use of a stringent threshold of 0.95 in Modkit identifies only ~55% of m^{5}C in the synthetic modified oligo, although it is fully modified.

To further consolidate this result, we assessed the presence of this modification in native DENV gRNA molecules and established a DENV-specific DRS approach. For this, three substantial challenges had to be overcome: (i) the length of DENV gRNA, (ii) the presence of complex secondary and tertiary structures within the gRNA [48, 49] that hamper passage through the nanopore, and (iii) the lack of a poly(A) tail to pull the gRNA through the nanopore. Thus, DENV gRNA was polyadenylated at the 3′ end *in vitro*, and complementary DNA oligonucleotides (Supplementary Table S1) were hybridized along the sequence to disrupt potential RNA structures prior to passing through the nanopore. To improve Dorado's basecalling accuracy for detecting m^5C sites during gRNA DRS, we trained the ONT basecaller using synthetic RNA oligonucleotides containing m^5C1218 in its native sequence context (mod, 100% methylation) alongside its unmodified counterpart (unmod) (Fig. 2D). These datasets allowed us to establish a stringent threshold that identifies modifications with over 95% probability and almost completely reduces false positives, albeit at the cost of underestimating m^5C modification levels in the fully modified synthetic oligonucleotide (∼55% detected instead of 100%) (Fig. 2E and Supplementary Table S2). In addition, sources of noise were reduced by analyzing three biological replicates of purified DENV gRNA and by comparative analysis with the unmethylated, similarly processed DENV full-length IVT. In line with the results obtained by BSSeq, DRS confirmed the presence of a single m^5C modification at position 1218 of DENV gRNA purified from infected cells, with an occurrence of ∼10% (Fig. 2E). As expected, given our strict thresholding, this occurrence was lower than that estimated by targeted MiSeq bisulfite sequencing (Fig. 2C).

Altogether, using complementary mapping methods and stringent analysis, we uncovered the presence of a single m^5C modification at position 1218 of DENV gRNA, at a frequency ranging between 10% and 20%. This occurrence aligns with the median level of m^5C methylation deposited by m^5C methyltransferases in human mRNAs, ranging from 15% to 18% [50, 51]. Notably, m^5C1218 is found exclusively in the cytoplasmic gRNA. This observation may suggest that mislocalized gRNA molecules may undergo methylation, or alternatively, that m^5C-modified gRNA molecules are selectively excluded from packaging into viral particles.

The host methyltransferase NSUN6 catalyzes DENV gRNA m^5C1218

The majority of m^5C modifications on mRNAs is catalyzed by the human methyltransferase NSUN2 [45], whose localization is mainly nuclear [35, 50]. Among the members of the NSUN family, NSUN6 is a cytosolic methyltransferase that primarily installs m^5C to the first cytosine of the consensus sequence motif CUCCA, often located in the loop of hairpin structures in mRNA 3′UTRs [45, 52, 53] and at the 3′ end of $tRNA^{Thr}$ and $tRNA^{Cys}$ at position 72 [54]. Supporting the possibility that this site is modified by NSUN6, inspection of the DENV gRNA sequence revealed that m^5C1218 coincided with the first cytosine of a CUCCA motif. We therefore investigated the potential role of NSUN6 in DENV gRNA methylation. Given that NSUN6 protein expression remained unchanged during infection (Fig. 3A), we generated Huh7 NSUN6 KO single-cell clones using the CRISPR/Cas9 technology and two guide RNAs targeting *NSUN6* locus at exons 1 and 3 (Supplementary Fig. S4A). Control cell clones were generated with a non-targeting guide RNA (NT) for comparison. Homozygous NSUN6 KO clones, validated by deletion of the endogenous locus and undetectable protein expression (Supplementary Fig. S4B), were pooled in equal numbers for all subsequent experiments to mitigate inherent variability among single-cell clones.

The m^5C modification affects several biological processes [55]. Therefore, we initially sought to assess the effect of NSUN6 depletion on processes that may indirectly influence the viral life cycle. First, we measured the levels of m^5C on $tRNA^{Thr}$, which is modified at position C72 by NSUN6 [54]. Of note, $tRNA^{Thr}$ is additionally methylated by NSUN2 in the tRNA variable loop (C48–50) [56, 57]. We used DORQ-seq, a hybridization-based approach that allows the purification of specific tRNAs [39], followed by LC-MS/MS (Fig. 3B). The m^5C levels on $tRNA^{Thr}$ isolated from Huh7 NSUN6 KO cells were reduced by ∼30% compared to those isolated from Huh7 NT cells. This result supported the role of NSUN6 in catalyzing one of three m^5C sites on $tRNA^{Thr}$ and suggested that NSUN6 deficiency did not alter the methylation of the other two sites by NSUN2. Moreover, depletion of NSUN6 had no significant effect on global translation (Fig. 3C) or cell growth (Supplementary Fig. S4C). Next, we examined a potential effect of NSUN6 depletion on DENV gRNA replication. For this, Huh7 NT and NSUN6 KO cells were electroporated with a full-length DENV firefly luciferase reporter RNA to bypass the natural entry pathway of the virus. Luciferase activity was used as readout for viral replication levels over time. Cells treated with NITD008, an adenosine nucleoside inhibitor that potently abrogates DENV replication [41], served as negative control (Fig. 3D). Similar replication levels were observed in Huh7 NT and NSUN6 KO cells, indicating that NSUN6 is dispensable for DENV gRNA replication (Fig. 3D).

To determine the direct involvement of NSUN6 in DENV gRNA m^5C1218 methylation, targeted MiSeq bisulfite sequencing was performed on total RNA extracted from infected Huh7 NT and NSUN6 KO cells (Fig. 3E), as well as RNA extracted from virions released in the respective supernatants (Supplementary Fig. S4D). In line with our earlier findings in infected parental Huh7 cells (Fig. 2A and B), m^5C1218 was identified in the gRNA extracted from Huh7 NT cells and undetectable in the gRNA extracted from the virions. In contrast, this modification was undetectable in the gRNA extracted from Huh7 NSUN6 KO cells (Fig. 3E), indicating a pivotal role for NSUN6 in catalyzing m^5C1218 in DENV gRNA in the cytoplasm.

Finally, we established an *in vitro* methylation assay using recombinant full-length NSUN6 and assessed the activity of NSUN6 on DENV RNA substrates (Fig. 3F). Recombinant full-length NSUN6 (Supplementary Fig. S4E) and ^3H-labeled S-adenosyl methionine (SAM) were incubated with 750 nM IVT of full-length DENV gRNA or IVT of DENV E coding sequence. Equal molarity of $tRNA^{Thr}$ was used as positive control. An IVT of the eGFP coding sequence that does not contain the CUCCA consensus motif was used as a negative control. As anticipated, NSUN6 was able to methylate $tRNA^{Thr}$. Both DENV RNA substrates were also methylated *in vitro* compared to the eGFP coding sequence (Fig. 3F), supporting the specific recognition of the CUCCA sequence by NSUN6 in the DENV gRNA sequence.

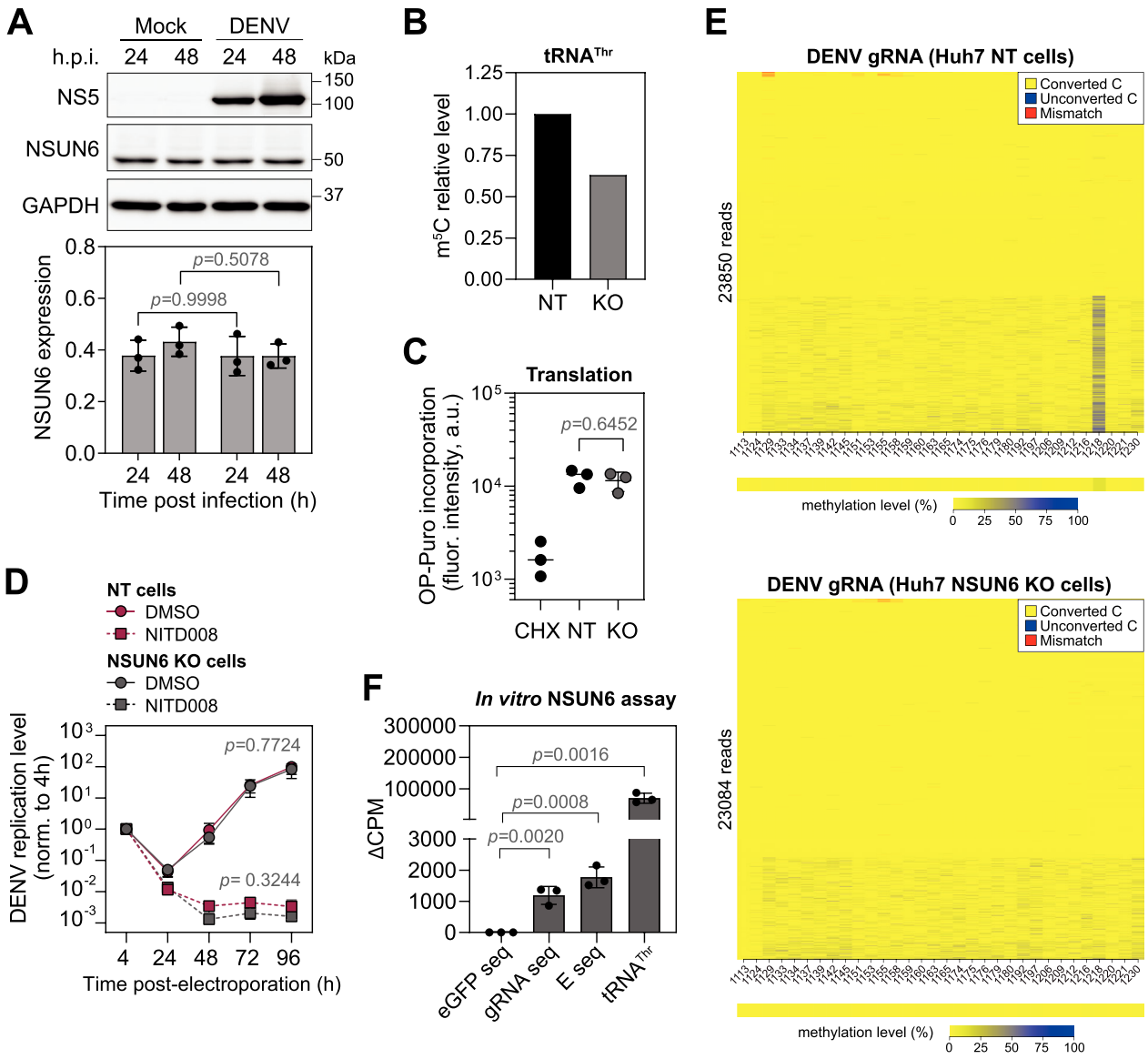

Figure 3. The host methyltransferase NSUN6 catalyzes DENV gRNA m^{5}C1218. (**A**) NSUN6 expression levels during DENV infection ($n = 3$). Shown is a representative immunoblot (top) and quantifications. DENV NS5 levels were normalized to the level of the loading control GAPDH (mean ± SD, $n = 3$). Statistical significance compared to the corresponding mock time point is indicated on the top. (**B**) Analysis of m^{5}C levels on tRNA^{Thr} in Huh7 NT and NSUN6 KO cells using the DORQ-seq approach followed by LC-MS/MS ($n = 1$). (**C**) Analysis of global translation levels in Huh7 NT and NSUN6 KO cells. Incorporation of fluorescently labeled OP-Puro was measured by flow cytometry. Cells treated for 1 h with cycloheximide (CHX) before OP-Puro incorporation were used as control for repressed translation. Shown is the mean fluorescence ± SD ($n = 3$). Statistical significance is indicated on the top. (**D**) Analysis of DENV replication in Huh7 NT and NSUN6 KO cells electroporated with DENV firefly luciferase reporter virus IVT ($n = 4$). Firefly luciferase activity was measured as surrogate for viral replication. Values were normalized to the 4 h time point to account for differences in electroporation efficiency. Cells treated with NITD008, a DENV RNA-dependent RNA polymerase inhibitor, served as control. Statistical significance compared to Huh7 NT cells is indicated on the top. (**E**) Analysis of m^{5}C methylation levels in gRNA extracted from infected Huh7 NT and NSUN6 KO cells using targeted MiSeq bisulfite sequencing ($n = 1$). Total RNA was extracted and submitted to bisulfite conversion before reverse transcription. An amplicon spanning DENV gRNA nt 1106 to 1266 was amplified by PCR and further processed for MiSeq. Shown are methylation heatmaps generated using BisAMP [36]. Each row corresponds to a sequencing read. Unconverted (i.e. methylated) cytosines are displayed in blue, while converted (i.e. unmethylated) cytosines are displayed in yellow. Mismatches to the reference sequence are displayed in red. Sequencing reads (23 850 for Huh7 NT; 23 084 for Huh7 NSUN6 KO) are aligned to the reference sequence and ordered from bottom to top according to their overall cytosine methylation level. The bars below the heatmap indicate the corresponding methylation level for each cytosine, expressed as the percentage of reads. This percentage is visualized using a color gradient from yellow (0, unmethylated cytosine residues) to blue (100, methylated cytosine residues). (**F**) NSUN6 *in vitro* methylation assay ($n = 3$). Recombinant NSUN6 was incubated with ^{3}H-labeled SAM and 750 nM of different DENV IVT substrates (DENV gRNA IVT and DENV E coding sequence IVT). An IVT of the eGFP coding sequence and tRNA^{Thr} were used as negative and positive controls, respectively. Shown is one representative experiment (mean of technical replicates ± SD). Statistical significance is indicated on the top.

NSUN6-mediated m^{5}C1218 destabilizes DENV gRNA

Among the different cellular processes, the m^{5}C modification influences mRNA turnover by promoting either degradation or stabilization, depending on the target mRNA [58–60]. We hypothesized a similar scenario for DENV gRNA and thus assessed the impact of NSUN6 on DENV gRNA turnover. Typically, the half-life ($t_{1/2}$) of cellular RNAs is determined by measuring RNA abundance after inhibition of transcription by actinomycin D treatment in time-course experiments. In contrast to cellular DNA-dependent RNA polymerases, DENV RNA-dependent RNA polymerase NS5 is not inhibited by actinomycin D. Thus, we adapted the approach and measured gRNA abundance following chemical inhibition of DENV gRNA synthesis using the NS5 inhibitor NITD008 [41] (see also Fig. 3D). To ensure sufficient replication and detectable gRNA levels by qRT-PCR, Huh7 NT or NSUN6 KO cells were infected with DENV for 24 h before inhibition of NS5 with NITD008 treatment. Cells treated with DMSO served as control. Cells were then harvested at 24-h intervals over a 5-day period. Strikingly, DENV gRNA $t_{1/2}$ increased from 40 h in Huh7 NT cells to ∼100 h in Huh7 NSUN6 KO cells, indicating that NSUN6 destabilizes DENV gRNA (Fig. 4A). This effect was also reflected by the slight increase of gRNA measured in Huh7 NSUN6 KO cells over time compared to Huh7 NT cells in the absence of NITD008 treatment (Fig. 4B).

To establish a direct causal relationship between m^{5}C1218 and DENV gRNA turnover, we generated a mutant virus containing a synonymous substitution at position 1218 (DENV C1218U) that disrupted the CUCCA motif. First, we assessed the impact of the mutation on viral replication using a full-length DENV firefly luciferase reporter virus (Fig. 4C). Both the WT and C1218U mutant viruses replicated to comparable levels, indicating that the mutation does not affect DENV gRNA abundance through changes in viral replication. Next, the half-lives of DENV WT and DENV C1218U gRNAs were determined in infected parental Huh7 cells, following the same procedure as previously established for the KO cells. Remarkably, the C1218U gRNA remained stable throughout the 96-h time course, while the WT gRNA exhibited a half-life of 53 h (Fig. 4D). Similar to the effect observed in Huh7 NSUN6 KO cells, the pronounced stabilization of the DENV C1218U gRNA resulted in its greater accumulation compared to the WT gRNA during infection (Fig. 4E), an effect not attributable to altered viral replication. We hypothesized that cytosolic accumulation of gRNA could promote virion assembly. To rule out potential confounding effects from cell death, we monitored cell death throughout the infection time course to identify the optimal time point for quantifying intracellular (assembled but unreleased) and extracellular (released in the supernatant) infectious particles (Fig. 4F). Cells continued to proliferate for up to 48 h after infection but showed pronounced cytopathic effects by 96 h, with comparable severity for both viruses. Therefore, viral titers were measured at 72 h, a time point coinciding with the observed accumulation of DENV gRNA (see Fig. 4D). Although the effect was less evident in extracellular particles, the moderate intracellular accumulation of C1218U gRNA in infected cells (see Fig. 4E) correlated with slightly higher levels of intracellular infectious DENV C1218U particles compared to WT (Fig. 4G). This result indicates that m^{5}C1218 ultimately reduces the pool of gRNA available for packaging into infectious virions.

Altogether, our findings reveal that NSUN6 catalyzes a highly specific m^{5}C modification at position 1218 of the DENV gRNA. This modification acts beyond the stage of replication as a critical regulatory mark that promotes DENV gRNA turnover, thereby limiting the pool of gRNA that can be packaged into viral particles and thereby progeny production.

Discussion

In this study, we have established ViREn, an approach to purify and enrich viral RNAs, which is ideally suited for profiling of RNA modifications using RNA sequencing-based approaches. We used DENV, a (+)ss RNA virus, as a model system, whose gRNA is over 10.7 kb long and not polyadenylated at its 3′ end. ViREn is a method that consists of two steps: (i) the removal of the most abundant and highly modified cellular RNAs based on the target RNA sedimentation coefficient in sucrose gradient ultracentrifugation and (ii) sequence-specific affinity capture of the target RNA. The sucrose gradient centrifugation also effectively removed intermediate-sized viral RNA species, detected using both northern blot 3′UTR and NS1 probes. These intermediates likely result from (i) 5′ to 3′ gRNA degradation by the exonuclease Xrn1, (ii) incomplete gRNA synthesis, or (iii) 3′ to 5′ degradation. While 3′ to 5′ degradation of flaviviral gRNAs is less documented than 5′ to 3′, recent studies show that the cellular 3′–5′ exonuclease ISG20 can degrade West Nile virus gRNA *in vitro*, but not the gRNA of Usutu virus, a closely related flavivirus [61]. DENV sfRNA was found to co-sediment across multiple gradient fractions, including fraction 11 containing gRNA, most likely due to its incorporation into high-molecular-weight complexes. Consequently, the second affinity-capture step was crucial to efficiently remove residual cellular RNAs and DENV sfRNA, thereby ensuring a highly purified gRNA preparation.

Despite modest yields after target RNA purification, ViREn achieved a significant reduction in background signals for Illumina-based RNA-seq and provided sufficient target RNA coverage to accurately identify RNA modifications in native gRNA molecules using DRS. Scale-up of starting material will allow the method to be combined with the use of LC-MS/MS to facilitate the detection of other RNA modifications not readily distinguishable with DRS using current basecaller algorithms. Finally, ViREn offers design versatility and straightforward transposability to other positive- and negative-sense ssRNA viruses as well as to cellular target RNAs. In the future, coupled with downstream detection methods, ViREn will facilitate the identification or validation of other RNA modifications such as m^{6}A, inosine, Nm, and pseudouridine.

Direct RNA sequencing of a 10.7 kb gRNA molecule with current nanopore technology remains challenging, especially for RNAs purified from cells. The ViREn approach proved essential for the reduction of cellular RNA and sfRNA contaminants, which would have otherwise occupied most of the sequencing pores and significantly limited the sequencing coverage of the DENV gRNA. Nevertheless, the success rate of passing the entire gRNA molecule through the sequencing pore was poor. We observed that the 3′ end stem-loop structure considerably hindered the entrance of the gRNA into the pore and a custom adapter directly targeting the 3′ end could not be efficiently ligated. This issue was addressed on the one hand by the addition of a poly(A) tail and on the other hand by using complementary oligonucleotides to disrupt the secondary

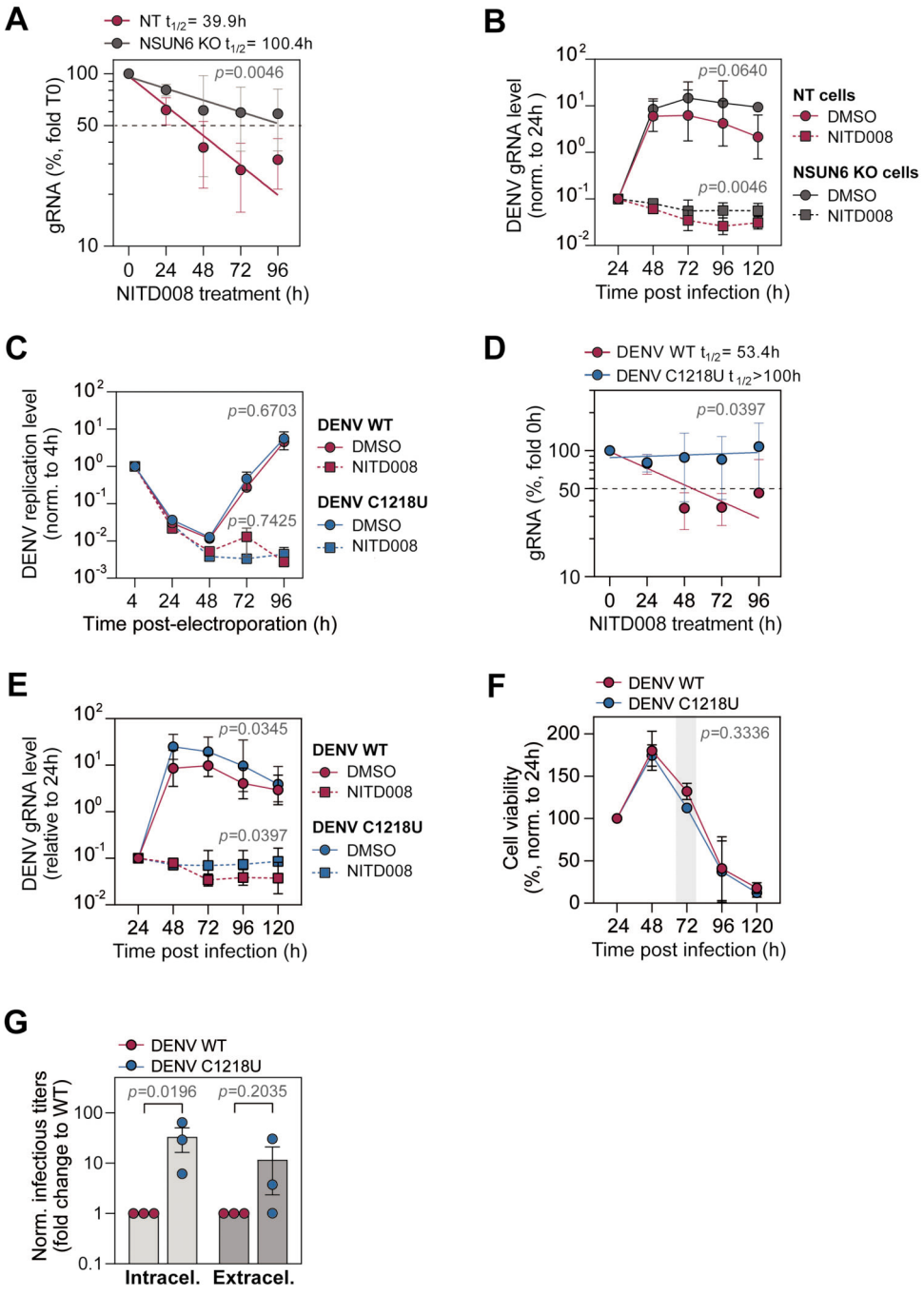

Figure 4. NSUN6-mediated m^{5}C1218 destabilizes DENV gRNA and restricts virion progeny production. (**A**, **B**) Measurement of DENV gRNA decay. Huh7 NT and NSUN6 KO cells were infected with DENV at an MOI of 0.1 for 24 h before treatment with the DENV replication inhibitor NITD008. (A) DENV gRNA levels were analyzed by qRT-PCR at indicated time points. Levels of DENV gRNA were normalized to *GAPDH* mRNA levels and to T0 (time of NITD008 addition). Shown are mean ± SD ($n = 3$). The half-life ($t_{1/2}$) of DENV gRNA was estimated from the decay curves. Statistical significance over all time points compared to Huh7 NT cells is indicated on the top. (B) Corresponding accumulation of DENV gRNA levels in Huh7 NT and NSUN6 KO cells over time ($n = 3$). Cells treated with NITD008 served as control. Cells were harvested at 24-h intervals and DENV gRNA was quantified by qRT-PCR (mean ± SD). Values were normalized to *GAPDH* mRNA levels and to time point 24 post infection. Statistical significance over all time points compared to Huh7 NT cells is indicated on the top. (**C**) The impact of m^{5}C on DENV replication was assessed using DENV2 NGC wildtype (WT) or C1218U firefly luciferase reporter virus (mean ± SD, $n = 3$). Huh7 cells were electroporated with DENV firefly luciferase reporter virus IVT. Firefly luciferase activity was measured as surrogate for viral replication at the indicated time points. Values were normalized to the 4 h time point to account for differences in electroporation efficiency. Cells treated with NITD008 served as control. Statistical significance compared to Huh7 NT cells is indicated on the top. (**D**–**G**) Huh7 cells were infected with DENV WT or DENV C1218U at an MOI of 0.1 for 24 h before treatment with the DENV replication inhibitor NITD008 ($n = 3$). (D) Measurement of DENV gRNA WT and C1218U gRNA decay in Huh7 cells (mean ± SD). Statistical significance over all time points compared to DENV WT is indicated on the top. (E) Corresponding DENV WT and DENV C1218U gRNA levels over time (mean ± SD). Statistical significance over all time points compared to DENV WT is indicated on the top. (F) Cell viability assay. The percentage of living cells after infection with DENV2 WT or C1218U was measured using the WST-1 assay at the indicated time points. Statistical significance compared to WT is indicated on the top. (G) Infectious titers of intracellular particles (extracted from cells) and extracellular particles (released in the supernatant). Virus was harvested at 72 h post infection (mean ± SEM) and normalized to time 24 h post infection. Statistical significance is indicated on the top.

structures present in DENV 3′UTR. The use of complementary oligonucleotides binding along the entire length of the gRNA led to improved sequencing throughput, presumably by disrupting more complex secondary and tertiary structures that appeared to be resistant to or able to refold after the various denaturation steps of the protocol.

Using stringent BSSeq, targeted MiSeq bisulfite sequencing, and DRS tailored to DENV gRNA, we identified and validated the presence of a single m^5C site at position 1218, in the E-coding sequence, in ∼10%–20% of DENV gRNA molecules. Consistent with its life cycle being exclusively cytoplasmic, our findings demonstrated that m^5C1218 is catalyzed by the host cytosolic methyltransferase NSUN6. As previously described for NSUN6-targeted mRNAs, the m^5C modification occurred on the first cytosine of a CUCCA consensus sequence motif within the DENV gRNA sequence. Using Huh7 NSUN6 KO cells and targeted MiSeq bisulfite sequencing, we confirmed the direct involvement of NSUN6 in the modification of DENV gRNA m^5C1218. The 10%–20% occurrence observed for the m^5C in DENV gRNA is similar to the median level of m^5C methylation in human mRNAs [50, 51]. Notably, *in silico* analysis of the DENV gRNA sequence revealed 16 CUCCA consensus sequence motifs, including one in the 3′UTR, a region in which the motif is more frequently modified in mRNAs [52]. Furthermore, while the position of this motif in the E coding sequence is conserved *in silico* in other DENV serotype 2 strains, e.g. 16 681, it is not conserved in the other three DENV serotypes. The DENV gRNA architecture is complex. SHAPE analyses of DENV gRNAs purified from viral particles have revealed numerous secondary and tertiary structures that vary between serotypes, as well as long-range interactions that are important for viral replication and virus fitness [48, 49, 62, 63]. We hypothesize that the CUCCA motif at C1218 in DENV2 NGC gRNA may be more accessible to the methyltransferase due to lack of tertiary structure, although other factors, such as nearby binding sites for RNA-binding proteins, may also contribute to modification selectivity. Whether m^5C modifications are present in other regions of the gRNA in different DENV serotypes and other flaviviruses will have to be investigated in the future.

The m^5C modification plays a role in several post-transcriptional RNA processes, including nuclear export, splicing, stability, and translation of mRNAs [55]. The deposition of m^5C is dynamic, and effects likely depend on the reader proteins that will recognize the modification [55]. These include Aly/REF export factor (ALYREF) [50], Y-Box binding protein 1 (YBX1) [58], LIN28B [64], YTH domain-containing family 2 (YTHDF2) [65], and serine/arginine-rich splicing factor 2 (SRSF2) [66]. For example, ALYREF promotes the nuclear export of the regulatory-associated protein of mTOR *RPTOR* mRNA [67], and YBX1 stabilizes the heparin-binding growth factor *HBGF* mRNA [58]. Conversely, the m^5C modification can also enhance mRNA decay, as observed for interferon regulatory factor 3 *IRF3* mRNA, resulting in a dampened interferon response during various viral infections [68]. By using a mutant virus with a synonymous substitution at position C1218, we have demonstrated that this single NSUN6-mediated m^5C modification promotes the degradation of the gRNA by a yet unknown mechanism. The stabilization of DENV C1218U gRNA was more pronounced than that of DENV WT gRNA in NSUN6 KO cells. Several factors may account for this difference. For instance, four NSUN6 KO single-cell clones were pooled per experiment. Biological variability among clones could attenuate the observed effect compared to experiments with DENV C1218U performed in the uniform wild-type Huh7 background. Additionally, known m^5C RNA reader proteins such as YBX1 and ALYREF can bind RNA even in the absence of m^5C modification. While we expect the m^5C methylation to increase affinity of the yet-unidentified reader protein, we cannot exclude that this reader protein can still bind the target sequence at position 1218 when unmodified. In contrast, the C1218U point mutation may eliminate the binding site entirely, preventing both methylation-dependent and -independent interactions. Such complete disruption of the reader interaction could lead to more severe changes than those caused by NSUN6 depletion. Interestingly, YBX1 was reported to act at different steps of the DENV viral cycle with opposite effects. While its binding to the 3′UTR negatively regulates viral replication [69], the interactions of YBX1 with the capsid and E proteins are necessary for the late steps of the viral life cycle, during the assembly of the viral particles [70, 71]. The identification of the m^5C reader protein will be important to elucidate the mechanism of DENV gRNA turnover.

In the absence of m^5C modification, DENV C1218U gRNA was markedly stabilized, leading to a moderate accumulation in infected cells compared to WT gRNA. Despite the technical challenges in quantifying small differences in infectious particles due to inherent assay variability, the level of infectious intracellular particles was significantly elevated. However, this was less evident for extracellular particles, although two out of three experiments showed the same tendency.

Emerging evidence indicates that NSUN2, a methyltransferase of the same family as NSUN6, methylates a variety of viral RNAs. For instance, viral RNAs of hepatitis B virus, a DNA virus that replicates in the nucleus are modified by NSUN2 at position 1291. The modification is recognized by ALYREF, which promotes export and translation of the viral mRNAs [72]. Recently, NSUN2 has also been reported to partially localize to the cytosol during infection with several (+)ssRNA viruses, where it modifies viral gRNAs. In HCV, a virus closely related to DENV, a single m^5C modification at position 7525 is recognized by YBX1 and increases gRNA stability and viral replication [73, 74]. In Enterovirus 71, multiple m^5C modifications increase gRNA stability and translation [75]. Conversely, the various m^5C modifications identified in the gRNA of severe acute respiratory syndrome coronavirus 2 promote its decay [76]. However, some of these results are being challenged [14] as the methods and rigor of the analyses improve.

Aligning with this observation and previously described limitations of RNA modification-specific antibody immunoprecipitation approaches [77, 78], our analysis of DENV gRNA DRS with Dorado 0.8.2, which also provides models for m^6A, did not identify any m^6A sites (Supplementary Table S2), also agreeing with recent antibody-independent SELECT analyses [13]. Taken together, these discrepancies underscore the importance of orthogonal validation to ascertain the presence of RNA modifications identified as well as their functional validation.

While the m^5C-modified gRNAs of the viruses mentioned above were also found in viral particles, the NSUN6-mediated m^5C1218 modification in DENV gRNA was exclusively detected in cytoplasmic gRNAs, but not in virions. This observation raises the possibility of a mechanism that prevents modified gRNAs from being packaged into viral particles. One

plausible explanation is that methylation serves as a quality–control mark, labeling mislocalized gRNAs for degradation, or alternatively, that methylated gRNAs are actively excluded through selective sorting processes. The mechanisms that determine how gRNAs are directed through different stages of the flaviviral life cycle remain poorly understood. It is tempting to speculate that different RNA modifications could serve as molecular markers that designate gRNAs for specific stages of the life cycle, such as replication, translation, degradation, or packaging. How DENV gRNA m^{5}C1218 is recognized, and the role of this modification in the DENV life cycle, remains to be elucidated.

Acknowledgements

We thank Sabine Wegehingel and Walter Nickel (Center for Biochemistry, Heidelberg University, Germany) for their assistance and access to the IncuCyte, and Bruno Sargueil (Université de Paris, France) for reanalyzing publicly available DENV2 gRNA SHAPE data. We are grateful to Laurent Chatel–Chaix (Centre Armand–Frappier Santé Biotechnologie, Canada) and to Oliver T. Fackler (Center for Integrative Infectious Disease Research, Heidelberg University, Germany) for helpful discussions and critical reading of the manuscript. We also acknowledge the Institute of Genetics and Biophysics A. Buzzati–Traverso. The National Research Council of Italy, for supporting Francesca Tuorto.

Author contributions: A.R. and M.H. conceptualized the study; C.C.W., I.S.N., J.H., Z.N., K.K., V.M., Z.Ö., D.L., S.S., and S.F. performed and analyzed experiments under the supervision of M.F., T.S., G.S., Y.M., F.T., C.D., M.H., and A.R.; J.S. analyzed the RNA-seq data. M.F., N.P., T.S., G.S., Y.M., F.T., C.D., M.H., and A.R.; C.C.W. and A.R. made the original draft of the manuscript. All authors edited and approved the final manuscript.

Supplementary data

Supplementary data is available at NAR online.

Conflict of interest

None declared.

Funding

This work was supported by the Deutsche Forschungsgemeinschaft (DFG, German Research Foundation) [project number 439669440 TRR319 RMaP A05 to A.R. and M.H., A04 to G.S. and N.P., A06 to F.T.; C02 to C.D.; project number 445549683 RTG2727 to J.S.]; and by the French Grand Est Region Project ViroMOD to Y.M. We also acknowledge Heidelberg University for the financial support of publication fees. Funding to pay the Open Access publication charges for this article was provided by Institutional core.

Data availability

- BSSeq data of DENV gRNA extracted from Huh7 cells and virions have been deposited at ENA (https://www.ebi.ac.uk/ena/) and will be publicly available as of the date of publication with the accession number PRJEB88116.
- DRS data of DENV gRNA and control sequences, as well as MiSeq sequencing data of DENV gRNA extracted from Huh7 cells, Huh7 NT and NSUN6 KO cells, and virions, have been deposited at NCBI SRA under the accession number SUB15204799.
- Illumina-based RNA-seq data of fraction 3 and fraction 11 before and after affinity capture has been deposited at NCBI GEO under the accession number GSE295911.
- All unique/stable reagents generated in this study are available upon request to the lead contact with a completed Materials Transfer Agreement.

References

1. Helm M, Motorin Y. Detecting RNA modifications in the epitranscriptome: predict and validate. *Nat Rev Genet* 2017;18:275–91. https://doi.org/10.1038/nrg.2016.169
2. Cappannini A, Ray A, Purta E *et al.* MODOMICS: a database of RNA modifications and related information. 2023 update. *Nucleic Acids Res* 2024;52:D239–44. https://doi.org/10.1093/nar/gkad1083
3. McCown PJ, Ruszkowska A, Kunkler CN *et al.* Naturally occurring modified ribonucleosides. *Wiley Interdiscip Rev RNA* 2020;11:e1595. https://doi.org/10.1002/wrna.1595
4. Sun H, Li K, Liu C *et al.* Regulation and functions of non-m^{6}A mRNA modifications. *Nat Rev Mol Cell Biol* 2023;24:714–31. https://doi.org/10.1038/s41580-023-00622-x
5. Boo SH, Kim YK. The emerging role of RNA modifications in the regulation of mRNA stability. *Exp Mol Med* 2020;52:400–8. https://doi.org/10.1038/s12276-020-0407-z
6. Huang G, Zhang F, Xie D *et al.* High-throughput profiling of RNA modifications by ultra-performance liquid chromatography coupled to complementary mass spectrometry: methods, quality control, and applications. *Talanta* 2023;263:124697. https://doi.org/10.1016/j.talanta.2023.124697
7. Herbert C, Valesyan S, Kist J *et al.* Analysis of RNA and its modifications. *Annu Rev Anal Chem (Palo Alto Calif)* 2024;17:47–68. https://doi.org/10.1146/annurev-anchem-061622-125954
8. Garalde DR, Snell EA, Jachimowicz D *et al.* Highly parallel direct RNA sequencing on an array of nanopores. *Nat Methods* 2018;15:201–6. https://doi.org/10.1038/nmeth.4577
9. Workman RE, Tang AD, Tang PS *et al.* Nanopore native RNA sequencing of a human poly(A) transcriptome. *Nat Methods* 2019;16:1297–305. https://doi.org/10.1038/s41592-019-0617-2
10. Gokhale NS, McIntyre ABR, McFadden MJ *et al.* N^6-Methyladenosine in flaviviridae viral RNA genomes regulates infection. *Cell Host Microbe* 2016;20:654–65. https://doi.org/10.1016/j.chom.2016.09.015
11. Lichinchi G, Zhao BS, Wu Y *et al.* Dynamics of human and viral RNA methylation during Zika Virus infection. *Cell Host Microbe* 2016;20:666–73. https://doi.org/10.1016/j.chom.2016.10.002
12. McIntyre W, Netzband R, Bonenfant G *et al.* Positive-sense RNA viruses reveal the complexity and dynamics of the cellular and viral epitranscriptomes during infection. *Nucleic Acids Res* 2018;46:5776–91. https://doi.org/10.1093/nar/gky029
13. Baquero-Perez B, Yonchev ID, Delgado-Tejedor A *et al.* N^6-Methyladenosine modification is not a general trait of viral RNA genomes. *Nat Commun* 2024;15:1964. https://doi.org/10.1038/s41467-024-46278-9
14. Huang A, Riepler L, Rieder D *et al.* No evidence for epitranscriptomic m^{5}C modification of SARS-CoV-2, HIV and MLV viral RNA. *RNA* 2023;29:756–63. https://doi.org/10.1261/rna.079549.122

15. Mazeaud C, Freppel W, Chatel-Chaix L. The multiples fates of the flavivirus RNA genome during pathogenesis. *Front Genet* 2018;9:595. https://doi.org/10.3389/fgene.2018.00595
16. Jones CI, Zabolotskaya MV, Newbury SF. The 5′ → 3′ exoribonuclease XRN1/Pacman and its functions in cellular processes and development. *Wiley Interdiscip Rev RNA* 2012;3:455–68. https://doi.org/10.1002/wrna.1109
17. Chapman EG, Costantino DA, Rabe JL *et al.* The structural basis of pathogenic subgenomic flavivirus RNA (sfRNA) production. *Science* 2014;344:307–10. https://doi.org/10.1126/science.1250897
18. Chapman EG, Moon SL, Wilusz J *et al.* RNA structures that resist degradation by Xrn1 produce a pathogenic Dengue virus RNA. *eLife* 2014;3:e01892. https://doi.org/10.7554/eLife.01892
19. Cumberworth SL, Clark JJ, Kohl A *et al.* Inhibition of type I interferon induction and signalling by mosquito-borne flaviviruses. *Cell Microbiol* 2017;19:e12737. https://doi.org/10.1111/cmi.12737 .
20. Manokaran G, Finol E, Wang C *et al.* Dengue subgenomic RNA binds TRIM25 to inhibit interferon expression for epidemiological fitness. *Science* 2015;350:217–21. https://doi.org/10.1126/science.aab3369
21. Moon SL, Dodd BJ, Brackney DE *et al.* Flavivirus sfRNA suppresses antiviral RNA interference in cultured cells and mosquitoes and directly interacts with the RNAi machinery. *Virology* 2015;485:322–9. https://doi.org/10.1016/j.virol.2015.08.009
22. Slonchak A, Khromykh AA. Subgenomic flaviviral RNAs: what do we know after the first decade of research. *Antiviral Res* 2018;159:13–25. https://doi.org/10.1016/j.antiviral.2018.09.006
23. Zhang Z, Jiang L, Zeng G. Non-coding RNA: a key regulator of the pathogenicity and immunity of Flaviviridae viruses infection. *Cell Mol Immunol* 2018;15:185–6. https://doi.org/10.1038/cmi.2017.86
24. Pijlman GP, Funk A, Kondratieva N *et al.* A highly structured, nuclease-resistant, noncoding RNA produced by flaviviruses is required for pathogenicity. *Cell Host Microbe* 2008;4:579–91. https://doi.org/10.1016/j.chom.2008.10.007
25. Liu-Wei W, van der Toorn W, Bohn P *et al.* Sequencing accuracy and systematic errors of nanopore direct RNA sequencing. *Bmc Genomics* 2024;25:528. https://doi.org/10.1186/s12864-024-10440-w
26. Gualano RC, Pryor MJ, Cauchi MR *et al.* Identification of a major determinant of mouse neurovirulence of dengue virus type 2 using stably cloned genomic-length cDNA. *J Gen Virol* 1998;79:437–46. https://doi.org/10.1099/0022-1317-79-3-437
27. Kumar A, Buhler S, Selisko B *et al.* Nuclear localization of dengue virus nonstructural protein 5 does not strictly correlate with efficient viral RNA replication and inhibition of type I interferon signaling. *J Virol* 2013;87:4545–57. https://doi.org/10.1128/JVI.03083-12
28. Roth H, Magg V, Uch F *et al.* Flavivirus infection uncouples translation suppression from cellular stress responses. *mBio* 2017;8:e02150–16.
29. van den Hoff MJ, Christoffels VM, Labruyere WT *et al.* Electrotransfection with "intracellular" buffer. *Methods Mol Biol* 1995;48:185–97.
30. Henchal EA, Gentry MK, McCown JM *et al.* Dengue virus-specific and flavivirus group determinants identified with monoclonal antibodies by indirect immunofluorescence. *Am J Trop Med Hyg* 1982;31:830–6. https://doi.org/10.4269/ajtmh.1982.31.830
31. Langmead B, Trapnell C, Pop M *et al.* Ultrafast and memory-efficient alignment of short DNA sequences to the human genome. *Genome Biol* 2009;10:R25. https://doi.org/10.1186/gb-2009-10-3-r25
32. Dobin A, Davis CA, Schlesinger F *et al.* STAR: ultrafast universal RNA-seq aligner. *Bioinformatics* 2013;29:15–21. https://doi.org/10.1093/bioinformatics/bts635
33. Liao Y, Smyth GK, Shi W. featureCounts: an efficient general purpose program for assigning sequence reads to genomic features. *Bioinformatics* 2014;30:923–30. https://doi.org/10.1093/bioinformatics/btt656
34. Thorvaldsdottir H, Robinson JT, Mesirov JP. Integrative genomics viewer (IGV): high-performance genomics data visualization and exploration. *Brief Bioinform* 2013;14:178–92. https://doi.org/10.1093/bib/bbs017
35. Dai Q, Ye C, Irkliyenko I *et al.* Ultrafast bisulfite sequencing detection of 5-methylcytosine in DNA and RNA. *Nat Biotechnol* 2024;42:1559–70. https://doi.org/10.1038/s41587-023-02034-w
36. Bormann F, Tuorto F, Cirzi C *et al.* BisAMP: a web-based pipeline for targeted RNA cytosine-5 methylation analysis. *Methods* 2019;156:121–7. https://doi.org/10.1016/j.ymeth.2018.10.013
37. Baek A, Lee GE, Golconda S *et al.* Single-molecule epitranscriptomic analysis of full-length HIV-1 RNAs reveals functional roles of site-specific m^6As. *Nat Microbiol* 2024;9:1340–55. https://doi.org/10.1038/s41564-024-01638-5
38. Magg V, Manetto A, Kopp K *et al.* Turnover of PPP1R15A mRNA encoding GADD34 controls responsiveness and adaptation to cellular stress. *Cell Rep* 2024;43:114069. https://doi.org/10.1016/j.celrep.2024.114069
39. Kristen M, Lander M, Kilz LM *et al.* DORQ-seq: high-throughput quantification of femtomol tRNA pools by combination of cDNA hybridization and deep sequencing. *Nucleic Acids Res* 2024;52:e89. https://doi.org/10.1093/nar/gkae765
40. Kellner S, Ochel A, Thuring K *et al.* Absolute and relative quantification of RNA modifications via biosynthetic isotopomers. *Nucleic Acids Res* 2014;42:e142. https://doi.org/10.1093/nar/gku733
41. Yin Z, Chen YL, Schul W *et al.* An adenosine nucleoside inhibitor of dengue virus. *Proc Natl Acad Sci USA* 2009;106:20435–9. https://doi.org/10.1073/pnas.0907010106
42. Livak KJ, Schmittgen TD. Analysis of relative gene expression data using real-time quantitative PCR and the $2^{-\Delta\Delta C_T}$ method. *Methods* 2001;25:402–8. https://doi.org/10.1006/meth.2001.1262
43. Stollar V, Stevens TM, Schlesinger RW. Studies on the nature of dengue viruses. II. Characterization of viral RNA and effects of inhibitors of RNA synthesis. *Virology* 1966;30:303–12. https://doi.org/10.1016/0042-6822(66)90105-X
44. Cleaves GR, Ryan TE, Schlesinger RW. Identification and characterization of type 2 dengue virus replicative intermediate and replicative form RNAs. *Virology* 1981;111:73–83. https://doi.org/10.1016/0042-6822(81)90654-1
45. Lu L, Zhang X, Zhou Y *et al.* Base-resolution m^5C profiling across the mammalian transcriptome by bisulfite-free enzyme-assisted chemical labeling approach. *Mol Cell* 2024;84:2984–3000.e8 https://doi.org/10.1016/j.molcel.2024.06.021e2988.
46. Schaefer M, Pollex T, Hanna K *et al.* RNA cytosine methylation analysis by bisulfite sequencing. *Nucleic Acids Res* 2009;37:e12. https://doi.org/10.1093/nar/gkn954
47. Motorin Y, Lyko F, Helm M. 5-methylcytosine in RNA: detection, enzymatic formation and biological functions. *Nucleic Acids Res* 2010;38:1415–30. https://doi.org/10.1093/nar/gkp1117
48. Dethoff EA, Boerneke MA, Gokhale NS *et al.* Pervasive tertiary structure in the dengue virus RNA genome. *Proc Natl Acad Sci USA* 2018;115:11513–8. https://doi.org/10.1073/pnas.1716689115
49. Boerneke MA, Gokhale NS, Horner SM *et al.* Structure-first identification of RNA elements that regulate dengue virus genome architecture and replication. *Proc Natl Acad Sci USA* 2023;120:e2217053120. https://doi.org/10.1073/pnas.2217053120
50. Yang X, Yang Y, Sun BF *et al.* 5-methylcytosine promotes mRNA export—NSUN2 as the methyltransferase and ALYREF as an m^5C reader. *Cell Res* 2017;27:606–25. https://doi.org/10.1038/cr.2017.55

51. Huang T, Chen W, Liu J *et al.* Genome-wide identification of mRNA 5-methylcytosine in mammals. *Nat Struct Mol Biol* 2019;26:380–8. https://doi.org/10.1038/s41594-019-0218-x
52. Selmi T, Hussain S, Dietmann S *et al.* Sequence- and structure-specific cytosine-5 mRNA methylation by NSUN6. *Nucleic Acids Res* 2021;49:1006–22. https://doi.org/10.1093/nar/gkaa1193
53. Liu J, Huang T, Zhang Y *et al.* Sequence- and structure-selective mRNA m^{5}C methylation by NSUN6 in animals. *Natl Sci Rev* 2021;8:nwaa273. https://doi.org/10.1093/nsr/nwaa273
54. Haag S, Warda AS, Kretschmer J *et al.* NSUN6 is a human RNA methyltransferase that catalyzes formation of m5C72 in specific tRNAs. *RNA* 2015;21:1532–43. https://doi.org/10.1261/rna.051524.115
55. Chen YS, Yang WL, Zhao YL *et al.* Dynamic transcriptomic m^5 C and its regulatory role in RNA processing. *Wiley Interdiscip Rev RNA* 2021;12:e1639. https://doi.org/10.1002/wrna.1639
56. Van Haute L, Lee SY, McCann BJ *et al.* NSUN2 introduces 5-methylcytosines in mammalian mitochondrial tRNAs. *Nucleic Acids Res* 2019;47:8720–33. https://doi.org/10.1093/nar/gkz559
57. Khoddami V, Cairns BR. Identification of direct targets and modified bases of RNA cytosine methyltransferases. *Nat Biotechnol* 2013;31:458–64. https://doi.org/10.1038/nbt.2566
58. Chen X, Li A, Sun BF *et al.* 5-methylcytosine promotes pathogenesis of bladder cancer through stabilizing mRNAs. *Nat Cell Biol* 2019;21:978–90. https://doi.org/10.1038/s41556-019-0361-y
59. Wu R, Sun C, Chen X *et al.* NSUN5/TET2-directed chromatin-associated RNA modification of 5-methylcytosine to 5-hydroxymethylcytosine governs glioma immune evasion. *Proc Natl Acad Sci USA* 2024;121:e2321611121.
60. Guarnacci M, Zhang PH, Kanchi M *et al.* Substrate diversity of NSUN enzymes and links of 5-methylcytosine to mRNA translation and turnover. *Life Sci Alliance* 2024;7:e202402613. https://doi.org/10.26508/lsa.202402613 .
61. Zoladek J, El Kazzi P, Caval V *et al.* A specific domain within the 3′ untranslated region of Usutu virus confers resistance to the exonuclease ISG20. *Nat Commun* 2024;15:8528. https://doi.org/10.1038/s41467-024-52870-w
62. de Borba L, Villordo SM, Iglesias NG *et al.* Overlapping local and long-range RNA–RNA interactions modulate dengue virus genome cyclization and replication. *J Virol* 2015;89:3430–7. https://doi.org/10.1128/JVI.02677-14
63. Huber RG, Lim XN, Ng WC *et al.* Structure mapping of dengue and Zika viruses reveals functional long-range interactions. *Nat Commun* 2019;10:1408. https://doi.org/10.1038/s41467-019-09391-8
64. Su J, Wu G, Ye Y *et al.* NSUN2-mediated RNA 5-methylcytosine promotes esophageal squamous cell carcinoma progression via LIN28B-dependent GRB2 mRNA stabilization. *Oncogene* 2021;40:5814–28. https://doi.org/10.1038/s41388-021-01978-0
65. Dai X, Gonzalez G, Li L *et al.* YTHDF2 binds to 5-methylcytosine in RNA and modulates the maturation of ribosomal RNA. *Anal Chem* 2020;92:1346–54. https://doi.org/10.1021/acs.analchem.9b04505
66. Ma HL, Bizet M, Soares Da Costa C *et al.* SRSF2 plays an unexpected role as reader of m^{5}C on mRNA, linking epitranscriptomics to cancer. *Mol Cell* 2023;83:4239–54.e10. https://doi.org/10.1016/j.molcel.2023.11.003
67. Zhong L, Wu J, Zhou B *et al.* ALYREF recruits ELAVL1 to promote colorectal tumorigenesis via facilitating RNA m^{5}C recognition and nuclear export. *NPJ Precis Oncol* 2024;8:243. https://doi.org/10.1038/s41698-024-00737-0
68. Wang H, Feng J, Zeng C *et al.* NSUN2-mediated m^{5}C methylation of IRF3 mRNA negatively regulates type I interferon responses during various viral infections. *Emerg Microbes Infect* 2023;12:2178238. https://doi.org/10.1080/22221751.2023.2178238
69. Paranjape SM, Harris E. Y box-binding protein-1 binds to the dengue virus 3′-untranslated region and mediates antiviral effects. *J Biol Chem* 2007;282:30497–508. https://doi.org/10.1074/jbc.M705755200
70. Diosa-Toro M, Kennedy DR, Chuo V *et al.* Y-box binding protein 1 interacts with dengue virus nucleocapsid and mediates viral assembly. *mBio* 2022;13:e0019622. https://doi.org/10.1128/mbio.00196-22
71. Phillips SL, Soderblom EJ, Bradrick SS *et al.* Identification of proteins bound to dengue viral RNA *in vivo* reveals new host proteins important for virus replication. *mBio* 2016;7:e01865–15. https://doi.org/10.1128/mBio.01865-15
72. Ding S, Liu H, Liu L. *et al.* Epigenetic addition of m^{5}C to HBV transcripts promotes viral replication and evasion of innate antiviral responses. *Cell Death Dis* 2024;15:39. https://doi.org/10.1038/s41419-023-06412-9
73. Li ZL, Xie Y, Wang Y *et al.* NSUN2-mediated HCV RNA m^{5}C methylation facilitates viral RNA stability and replication. *Genomics Proteomics Bioinformatics* 2025;23:qzaf008. https://doi.org/10.1093/gpbjnl/qzaf008
74. Li ZL, Xie Y, Xie Y *et al.* HCV 5-methylcytosine enhances viral RNA replication through interaction with m^{5}C reader YBX1. *ACS Chem Biol* 2024;19:1648–60. https://doi.org/10.1021/acschembio.4c00322
75. Liu L, Chen Z, Zhang K. *et al.* NSUN2 mediates distinct pathways to regulate enterovirus 71 replication. *Virologica Sinica* 2024;39:574–86. https://doi.org/10.1016/j.virs.2024.05.002
76. Wang H, Feng J, Fu Z *et al.* Epitranscriptomic m^{5}C methylation of SARS-CoV-2 RNA regulates viral replication and the virulence of progeny viruses in the new infection. *Sci Adv* 2024;10:eadn9519. https://doi.org/10.1126/sciadv.adn9519
77. McIntyre ABR, Gokhale NS, Cerchietti L *et al.* Limits in the detection of m^{6}A changes using MeRIP/m^{6}A-seq. *Sci Rep* 2020;10:6590. https://doi.org/10.1038/s41598-020-63355-3
78. Helm M, Lyko F, Motorin Y. Limited antibody specificity compromises epitranscriptomic analyses. *Nat Commun* 2019;10:5669. https://doi.org/10.1038/s41467-019-13684-3

Received: April 18, 2025. **Revised:** December 15, 2025. **Accepted:** December 23, 2025